UCRL-11067

University of California

Ernest O. Lawrence Radiation Laboratory

MODERN METALLOGRAPHIC TECHNIQUES

Berkeley, California

DISCLAIMER

Rept. submitted for presentation in the Aerospace Materials Conf. – Nov. 11, 1963, Los Angelas, Calif.

Rept. also submitted for publication in the Proceedings.

UCRL-11067

UNIVERSITY OF CALIFORNIA

Lawrence Radiation Laboratory
Berkeley, California

AEC Contract No. W-7405-eng-48

MODERN METALLOGRAPHIC TECHNIQUES

G. Thomas

November 8, 1963

UCRL-11067

MODERN METALLOGRAPHIC TECHNIQUES

G. Thomas

Inorganic Materials Research Division, Lawrence Radiation Laboratory
and Department of Mineral Technology, University of California
Berkeley, California

Paper to be presented at Conference on Aerospace Materials - Nov. 1963
Los Angeles, to be published.

November 8, 1963

1. Introduction

Metallography is the branch of metallurgy which is concerned with the study of structure and constitution of solid metals and alloys and its relation to the properties of these materials and also to their manufacture and treatment.

The structure of materials can be studied directly by various microscopical methods. The ability to resolve features of the structure depends on the wavelength of the illumination used and the efficiency of the optical system, i.e., the perfection of the lenses used in the microscope. The resolvable separation d of two objects is given by the well known optical relationship

$$d = \frac{0.61\,\lambda}{\mu \sin \alpha} = \frac{0.61\,\lambda}{N}$$

Where d = wavelength, μ = refractive index, and $\mu \sin \alpha = N$ is the numerical aperture of the lens. To improve resolution it is obvious that λ should be made as small as possible and N as large as possible. For light optics the following resolutions can be obtained:

white light, λ = 4200 Å	N = 1.4 (oil immersion)	d = 1800 Å
ultraviolet light, λ = 2537 Å	N = 1.4	d = 1100 Å

The optimum resolution in light optics is thus ~1000 Å. Smaller wavelengths are possible by using x-rays and electrons. In the former case lenses for refracting x-rays are impractical but in the latter case electromagnetic or electrostatic lenses can be used to focus electron beams. Unfortunately electron lenses cannot be made with large aperture

systems and in practice the effective aperture of an objective lens is ~10^{-2} to 10^{-3} radians. This small value is used in order to minimize the four most important sources of error in the image: diffraction error, spherical aberration, astigmatism and chromatic aberration. As a result, even for electron wavelengths as small as 0.037 Å (100 KV electrons), the optimum resolution in electron microscopy is ~ 4Å which is insufficient for atomic resolution. The only imaging system capable of resolving atoms is the field ion microscope.

Although for many purposes a high power microscope is essential to the metallographer, some obvious structural features can be observed by eye or with the use of a low power hand lens. Such macrostructural details include cracks, porosity, segregation in castings, grain size, fracture characteristics and flow lines in forgings or extrusions, etc. The Magnaflux and Magnaglo processes are extremely useful for detecting small macroscopically invisible surface flaws which may be dangerous. In the former method magnetic particles are made to collect at discontinuities in the surface. For non-magnetic materials a dye containing oil is allowed to penetrate into the cracks (Magnaglo Process) and are visible under ultraviolet light because then the dye fluoresces. Various non-destructive techniques can also be used for detecting internal flaws, e.g., by ultrasonic testing.

This year (1963) marks the Sorby Centennial.* Sorby has become known as the father of metallography although much of his work was done using the polarizing microscope for petrographic studies. Figure 1 is an example

* The Society for the History of Technology is publishing a book describing the work of Sorby and others who have done so much to establish Metallurigcal Science (to be published by Gordon & Beach Science Publishers on behalf of the A.I.M.E.).

of an historical, but still beautiful micrograph, taken by Wildmanstatten from a meteorite. Widmanstatten's name now adorns all microstructures in which precipitated phases are crystallographically related to the parent crystal.

The usefulness of the light microscope has now been well demonstrated but many properties were not explained by what could be seen in this instrument. Indirect structural determinations were made using x-ray diffraction techniques and for example, Guinier and Preston in 1938 showed that age-hardening in aluminum alloys was due to precipitation of the, then, invisible very small phases. The term substructure then became used to describe structure not resolved by the light microscope. The mechanical behavior of metals was explained qualitatively by the theory of dislocations as long ago as 1932, but dislocations were not resolved until quite recently when x-ray and electron microscopy techniques were developed. In the latest phases of metallography the development of the field ion microscopy has now enabled the individual atom to be resolved.

It is the object of this paper to describe generally but briefly the latest techniques which are available for direct structural observations. All I can do here is to hint at the type of work that is being done and the reader should not be misled by my brief descriptions. The references given are typical but not exhaustive, since the literature describing each single technique and its applications is now voluminous. Etch pit techniques, electron and x-ray microscopy, thermionic emission and field ion microscopy, and probe microanalysis only will be considered here.

2. Optical Metallography

For over seventy years, the light microscope has proved to be immensely valuable in understanding the structure of many materials but unfortunately since the best resolution obtainable is ~1100Å most of the important substructural features in metals, e.g., dislocations, small particles, etc., are not observable. Recent reviews of metallographic techniques for light microscopy are given in Ref. 1.

Figure 2 shows the structure after deformation of a steel containing martensite and retained austenite (a) polished prior to deformation. After repolishing (b) the slip lines in the austenite have been removed but the deformation markings in the martensite remain. This simple but elegant demonstration shows that this type of martensite deforms by mechanical twinning. In low carbon steels, however, the martensite deforms by slip. Recent work using transmission electron microscopy (see Section 6) has shown that in the former case the martensite contains very fine transformation twins not resolvable in the light microscope. This is an example where the combination of light and electron microscopy is extremely valuable in helping to understand complex phenomena.

In modern times the light microscope has been used to study dislocations in crystals by means of the etch pit technique. The development of the method owes much to the pioneering efforts of Vogel et. al[2] who established a one-to-one correspondence between etch pits and dislocations in germanium. Regel et. al,[3] Johnston,[4] Forty[5] and Mitchell[6] have reviewed etch pitting techniques. Proceedures and techniques are described in the former two references.[3, 4] In the etch pit method it is necessary to find a chemical solution which preferentially attacks

places at the surface where dislocations emerge. Often only certain crystallographic faces respond to the etchant. Dash[7] found that all faces could be etched in silicon samples if they were left overnight in a solution of 1 part HF, 3 parts HNO_3 and 10 parts glacial acetic acid. Figure 3 is an example of etch pits at isolated dislocations and dislocations in slip bands in a crystal of MgO.

In metallurgical research considerable attention is being paid to the behavior of bcc metals in order to understand yielding behavior. Since it appears that the yield phenomenon is related to the number and velocity of mobile dislocations[8] estimates of these numbers are needed. Table I gives a comparison of the methods (and their imitations) whereby dislocation densities can be estimated. The classical etch-pit experiments of Low et. al[9, 10] demonstrated the velocity - stress dependence of dislocations in iron.

Washburn[11] has made some criticisms of the etch-pit method. For example, a count of dislocation etch pits in a slip band usually has no relation to the number of moving dislocations. This is because the pits denote immobile dislocations in the form of loops and dipoles. Figure 4 is an electron micrograph of MgO showing numerous loops and dipoles.[12] The density of pits also has nothing to do with the shear strain in the band, since the latter is determined by the number of dislocations that have traversed the slip planes and left the crystal, and is not necessarily related to the debris left behind.

Although it was thought that etch pits could only be formed at dislocations which had impurities associated with them it is now believed that "clean" dislocations can also be revealed (see Ref. 6). Decoration

Table 1

The Methods for Estimating

Maximum Dislocation Densities*

Technique	Spec. Thickness	Width of Image	Maximum Density
Electron Microscopy	must be > 1000 Å (**)	~ 100 Å	10^{11} - 10^{12}/cm^2
X-ray Transmission	0.1-1.0 mm	5μ	10^4 - 10^5
X-ray Reflection	< 2μ (min.) - 50μ (max.)	2μ	10^6 - 10^7
Decoration	~10μ (depth of focus)	0.5μ	2 x 10^7
Etch-Pits	no limit	0.5μ+	4 x 10^8

* Based on W. G. Johnston.(4)

+ Optical limit of resolution of etch-pits.

** In very thin foils dislocations may be lost as a result of thinning. For 100 kV operation 5,000 Å is about the upper limit of transparency for most metals.

of dislocations by precipitates enables them to be observed in transparent crystals[7] and in metals by replication techniques.[13] (see Fig. 14).

The etch-pit method is powerful, rapid and non-destructive. Dislocations can be revealed by applying stresses after etch pits have been formed and then located in their new positions by a further etch. The main limitations are knowing whether all pits always correspond to dislocations. The ability to produce dislocation etching depends critically upon the orientation and state of the specimen surface and on the precise composition of the etchant. Pits are not formed on low index faces which dissolve at the highest rates in a particular etchant, and the shape, resolution and size of pits depends on the nature and concentration of the controlling impurity, e.g., bromide ions for copper etches. If the density of dislocations is much above 10^8 interactions between overlapping pits renders resolution of individual pits difficult if not impossible. Surface replication and examination in the electron microscope is helpful under these circumstances. Ideally all the methods shown in Table I should be used on the same specimen if the most reliable information is to be obtained.

3. X-Ray Microscopy

Since x-rays have greater penetration into matter than either light or electrons microstructural features can be investigated in opague specimens. However, there are difficulties in making x-ray microscopes in that lenses for refracting x-rays are impractical.[14] Projection microscopes have been utilized for mostly biological work but some

applications to segregation and alloy structures have been carried out.[15, 16] Direct x-ray magnification is obtained by placing the sample close to the x-ray source and the photographic plate some distance away. For a magnification of 100x in a camera of length 10 cm. the sample is 1 mm. from the source.[14] When the sample is placed next to the photographic plate contact microradiographs are obtained. In this case there is a 1:1 magnification. Both methods rely upon the relative absorption of x-rays from areas of the specimen containing different elements. Since microgradiography and projection microscopy have been considered in great detail elsewhere[14-17] no further mention of these techniques will be made here.

X-ray diffraction micrographs are now being obtained which resolve substructure in materials, including individual dislocations. The technique has some advantages over electron microscopy and etch pit methods in that the specimen can be observed non-destructively and without subject to damage. Also thick specimens can be studied. Two main techniques are employed, viz,, the Berg-Barrett[18, 19] and the Lang[20] methods. The former is simple and inexpensive whereas the latter requires more complex apparatus, thinner crystals and long exposure times for photography.

The principle of the two methods is shown in the sketches of Fig. 5. The methods rely upon diffraction of x-rays whenever Bragg's law: $2d \sin \Theta = \lambda$ is satisfied. Since the images are formed of the diffracted beams they are dark field images. The Berg-Barrett method can be used for thicker crystals by taking reflecting photographs (Fig. 5b) and both techniques (Fig. 5a,c) are suitable for transmission work.

Transmission Berg-Barrett

Parallel x-ray beams from a linear x-ray source are used so that a photograph of a given width of crystal can be obtained with only one exposure. An ordinary sealed-off x-ray tube is sufficient as the source. Since it is difficult to remove the K_{α_2} lines the resolution is limited by the dispersion of K_{α_1} and K_{α_2}. For example, when a focus of 1 mm. length horizontally and 0.5 mm. width vertically is used and the source-specimen distance is 50 cm., the specimen-plate distance is 1 cm., the resolution is 10μ and 7μ respectively in the normal and parallel directions using MoK_{α} reflected by (111) silicon.

A number of investigations have been reported.[15, 21, 22, 23] Newkirk[23] has summarized the use of the Berg-Barrett method for observing imperfections and Fig. 6a is an example of a reconstructed LiF crystal from several x-ray micrographs showing slip lines, sub-grains and grown-in dislocations. Figure 6b shows a comparison of an optical and a diffraction micrograph from the same area of a Fe-4% Si crystal. The correspondence between the two is clear.

Lang Method

As shown in Fig. 5a if a point focus x-ray source (characteristic radiation) is used the K_{α_1} line only can be used to illuminate the specimen. After diffraction, the diffracted beams only reach the photographic plate (placed normal to the beam) since the transmitted beam is stopped by the slit S_2. In order to obtain a projected image over a wide area of the specimen both the crystal and plate are simultaneously moved to the left and right. The images of each area

are thus recorded continuously. In both techniques the images are magnified optically for observation. The resolution possible with this arrangement is ~0.5μ. In obtaining images of dislocations, the resolution of the camera should be ~1μ giving an image width of 10-50 μ. For this reason investigations can only be carried out on crystals with a relatively low dislocation density ($10^8/cm^2$ or less). Lang cameras are made commercially.

Determination of Burgers Vectors of Dislocations

As will be seen in Section 6 (Fig.20) a defect whose displacement vector $\vec{R}$ lies parallel to the reflecting plane does not change the direction of the diffracted beam and so the defect is then invisible. Since the reciprocal lattice vector is normal to the reflecting plane the criterion for visibility is thus $\vec{g}\cdot\vec{R} \neq 0$. Thus by examining different reflections and noting that when $\vec{g}\cdot\vec{R} \neq 0$ the direction of $\vec{R}$ can be determined (see Fig. 21). However, the image is relatively insensitive to the sign of $\vec{R}$, so for dislocations only the direction of the Burgers vector can be determined. Examples of the use of this method can be found in Refs. 7, 20, 21 and 23.

4. Thermionic Emission Microscopy

The thermionic emission microscope represents one of the first types of electron microscope ever used.[24] Since high temperatures are often required to obtain thermiomic emission the technique is not suitable for biological and medical research and has not been used for metallurgical studies until quite recently.[25-29].

In order to obtain electron emission from the specimen the following must be achieved: (1) reduce the work function of the metal and/or (2) raise the energy level of the electrons and/or (3) reduce the potential barrier. All three methods are used in practice to increase the probability of electron escape from the metal surface. The work function of the metal is lowered by activation with barium or strontium carbonate. An accelerating voltage of 20-50 kV is applied to reduce the potential barrier, and by heating the specimen, enough thermal energy is supplied so that electrons can leave the metal.[30] The specimen itself is used as the electron source and is in the form of a flat sheet. The emitted electrons are accelerated by the electrical field and focussed by either an electrostatic or an electromagnetic lens, which forms the image of the specimen surface on a phosphorescent screen. A photograph and a section of a typical microscope is shown in Fig. 7.

The minimum operating temperature in order to obtain a satisfactory picture, if surface activation with barium carbonate is used, is about 450°C.[7] The picture one obtains is exactly like a metallographic one but the resolution obtainable (~500 Å) and the contrast is considerably better than in a light optical image. Furthermore, dynamic events can be followed, by using movie camera techniques so that precipitation, recrystallization, etc., all can be studied directly, provided the phenomenon occurs at a temperature in excess of that required to obtain emission.

The contrast in the image depends upon the relative emission from various parts of the specimen. The emission is orientation dependent so that individual grains show different intensities; solute atoms can increase or decrease the emission. For example, carbon and copper in

iron increases emission while chromium and silicon in iron decreases the emission. Stress concentrations or gradients also affect the emission.

Figure 8 is taken from a movie film showing the γ-α transformation in pure iron. The twins in the γ phase are clearly resolved (Eichen, priv. comm.). The specimen has been activated with barium carbonate. The potentialities of the technique are great and the following is a list of some possible investigations which can be carried out:(30)

1. Phase transformation, phase boundary-temperature relations
2. Recrystallization and grain growth
3. Cold work
4. Creep
5. Diffusion
6. Segregation
7. Solidification
8. Surface adsorption and other surface reactions
9. Electron emission; measurement of work function.

An important recent development in thermionic emission microscopy is surface activation with ions (Duker, priv. comm.). The electron emission is obtained by energy inparted to the specimen from an impinging beam of high energy ions accelerated from an ion gun. The advantages of this technique are:

1) The surface is kept clean by ion bombardment.
2) No activating substance need be used on the specimen surface.
3) Operation at as low as room temperature is possible.
4) Gases can be selected so as to produce chemical environments which enalbe oxidation and corrosion phenomena to be studied directly.

The ion activated electron emission microscope is termed the metioscope and is now being manufactured in Switzerland.

5. Field-Ion Microscopy

This type of microscopy is a newer version of the older field emission microscope in which the image of a hemispherical surface of a finely pointed specimen is radially projected onto a phosphor screen by electrons emitted under an applied field.[31] The resolution is limited to ~30 Å and as such is inferior to the electron microscope. However, in 1951, Müller[32] succeeded in resolving the individual atom by imaging the fine tip with ions produced by field ionization of He (or Ne) gas at a field of 450-350 MV/cm. The field ion microscope thus has the highest resolution of any known imaging instrument.

A schematic sketch of the microscope is shown in Fig. 9. The metal specimen is in the form of a fine wire electropolished at one end to obtain a sharp hemispherical tip of ~300 atoms or less in radius. The specimen is welded at the opposite end to a filament between tungsten electrodes which are cooled in liquid nitrogen or hydrogen. For tip radii < 500 Å liquid nitrogen is a sufficiently good coolant to give atomic resolution. The specimen is changed relative to the screen to a positive potential of 5 to 15 kV. As shown in the figure straight lines of electrostatic force thus run radially from the tip to the screen. In the field emission microscope the tip is negatively charged so that the image is formed of those electrons which reach the screen. However, since these electrons are emitted with appreciable velocities normal to the lines of force, the image is blurred and there is loss in resolution.

By positively charging the tip, the free electron cloud is pushed slightly into the metal os that positively charged metal ions are carried to the screen by a gas atom (He or Ne). The gas atom on raching the tip gives up an electron to the metal and becomes a positive ion. Under the field of force this ion is accelerated along the line of force and produces an image at the point it hits the screen. The image obtained is thus one of bright spots each corresponding to the helium ions emanating from each ionization center on the surface. The clearest atoms seen are those in exposed positions, e.g., at edges of planes or in the faces of high index planes (see Fig. 10).

A critical condition for atomic resolution is that surface contamination at the tip must be avoided. A unique feature of the He or Ne operated field ion microscope is that under imaging conditions, because of the high ionization potential required for He atoms, other gaseous atoms ionize before they reach the specimen and therefore do not contribute to the image. Thus the tip does not become contaminated by impurities in the gas. The specimen can therefore be kept atomically clean with only modest vacuum requirements.[33] The impairing effect of thermal vibrations on the atomic resolution is minimized by operating at the low temperatures.

Field desorption and field evaporation serves to clean the specimen surface in situ at low temperatures. Furthermore, surface atoms can be removed layer by layer by field evaporation in a controlled way. As a result missing atoms, i.e., vacancies can be counted directly. Figure 10 is an example of a platinum image in which missing atoms can be seen at various places.[34]

Field evaporation limits the applicability of the F.I.M. to high melting point metals since the evaporation field must be greater than

the imaging field. Iron, cobalt and nickel lie at the limit for helium ion images. Neon images will make it possible to resolve atoms in lower melting point metals but since the image brightness for Ne is ~20 times smaller than for He it is essential to employ an image intensifier. Without intensifiers, a helium ion current ~ 10^{-9} amp enables a photograph to be obtained after several minutes exposure.

The magnification of the image is ~ screen-tip distance/tip radius, i.e., about one million. The image consists of dome-like regions of a stack of concentric desks, and from its pattern the orientation and crystallographic character of the features can be determined (Figs. 10, 11).

The specimen itself is subjected to stresses ~ 1 ton/mm^2 for an applied field of 450 MV/cm. This is perhaps one of the serious disadvantages of the technique, since all specimens are observed under this high stress. Since the atoms in metals are resolved, vacancies, interstitials, impurity atoms, segregation, order, dislocations, grain boundaries, etc., can all be observed directly (see Refs. 35-37 for reviews of applications). Figure 11 shows examples of interstitial damage (arrowed) produced by α-particle irradiation of tungsten. Müller[35] suggests that the large bright spots in the image are due to the following. The lattice strain surrounding the interstitial relaxes when the defect isjust below the first surface layer. This area is then rearranged to form a hump of atoms with reduced coordination causing a bright large spot to appear in the ion image. However, many of the contrast effects observed in field ion images are not yet completely understood. Recently Brandon and Wald[38] were able to follow directly the production of point defects by ion bombardment of tungsten specimens inside the microscope.

The field ion microscope is very promising and when a wider range of metals can be examined more people will undoubtedly start to use the technique. Since the atomic structure can be directly resolved the method should be very useful for distinguishing between local order and clustering and other effects which cannot be resolved by any other means.

6. Electron Microscopy

The optical arrangement of lenses in an electron microscope is similar to that in the light microscope as shown in Fig. 12. In modern instruments the lenses are electromagnetic and because high currents are often used in the lens coils, the lenses may be water cooled. The electron source is a fine tungsten wire which when heated to > 1000°C emits electrons. These are then accelerated at -40 to -150 KV (depending on the instrument) through an anode at ground potential. A pair of condenser lenses then narrows the beam such that a minimum spot diameter of ~2μ is possible at the specimen. In this way the fine focus high intensity beam enables better transmission through metal foils to be attained than if a single condenser lens is used. Also, double condensers minimize thermal overloading of the specimen due to beam heating. The objective lens usually of small focal length (~3 mm.), projects an magnified image of the object onto the front focal plane of the projector. Usually a total of three stage magnification is obtained by the use of an intermediate and a projector lens after the objective. If the specimen is crystalline a diffraction image is formed at the back focal plane of the objective (Fig. 13). When the intermediate lens is defocussed to zero magnification the diffraction pattern can be displayed at the fluorescent screen. By

increasing the current in the intermediate lens an image of this pattern can be formed at the screen. Thus selected area diffraction patterns can be obtained from different places in the specimen and contrast arises primarily through diffraction. In amorphous films (e.g., replicas) most of the contrast arises from mass thickness scattering so that thick areas will appear darker than thin areas.

One of the major advantages of electron microscopy is the great resolution possible (~4 Å) and because the depths of field and focus are very large. Thus a focussed image at the screen is also in focus at the photographic plate position (below the fluorescent screen). A 35 mm. camera can also be positioned above the screen for use when a large number of photographs need to be recorded with the minimum of time. Since the penetration of electrons through materials is limited, very thin specimens must be used. Nowadays techniques are available for preparing thin sections of almost any material that needs to be examined.[39, 40] However, the correlation of microstructure in thin films with bulk properties must be made with some reservations particularly with regard to dislocation behavior, e.g., because of possible rearrangements during thinning. Furthermore, since only a small volume of material is examined from a given specimen adquate sampling must be carried out. In order to make quantitative measurements, e.g., dislocation density or volume fraction of precipitates, it is essential to know the foil thickness. The latter can be found from a known trace, e.g., slip traces, twin traces, etc. The trace is projected in the micrograph so that the foil orientation must be determined from the diffraction pattern in order to know the angle between the plane of the trace and the foil surface.

Replica Methods

The earliest application of electron microscopy to metallurgical research involved surface replication.[39-43] The usual replicas now used are carbon or SiO, while for Al and its alloys their own oxide film can be used. The metal surface is covered with a replicating medium of 200-500 Å thickness. In the case of C and SiO films these are produced by vacuum evaporation after the specimen has been prepared metallographically in the usual way. Oxide films on aluminum and its alloys are produced by anodising the surface. Second phase particles usually do not form a coherent oxide film so that holes at these regions in the replica delineate such particles. As example for an Al-4% Cu alloy is shown in Fig. 14. The replicas must be detached chemically from the metal by electrolytic polishing or etching (see, e.g., Ref. 39). In the case of ferrous materials since precipitates are cathodic with respect to the matrix etching through the film allows particles to be extracted in the replica.[3] An example of extracted chromium carbide particles from a low alloy tempered steel is shown in Fig. 15. These extracts can be examined by fluorescent analysis (e.g., in the probe section) in order to obtain information regarding their composition. Also since they are crystalline the selected area diffraction technique may be used to distinguish between the various phases which may be present, as well as to obtain structural information (Fig. 15b).

The maximum resolution possible with replicas is ~20 Å. The replica technique has been widely used to study surface features associated with slip (Fig. 6), precipitation phenomena, fracture, etc., (see, e.g., Refs. 39, 43, 44, 45). However, with the advent of thin foil techniques and the development of better microscopes, replica methods are now being superceeded.

Thin Foils

Transmission electron microscopy of thin foils is now the most widely used of the modern metallographic techniques. The tremendously rapid growth of the method over the past ten years[39, 44, 46-48] is mainly due to:

(1) Development of techniques for preparing specimens thin enough to be transparent to electrons (< 0.5μ).

(2) The availability of electron microscopes with double condenser lens systems, selected area diffraction and high voltage facilities.

(3) Development and application of the theory of electron diffraction which facilitates the interpretation of the often complex images observed.

Because of the low penetration of electrons through matter, specimens have to be prepared about 2000 Å thick in order to obtain transmission.[39, 40] Reflection electron microscopy does not require thin specimens but due to the poorer resolution possible (~80 Å compared to say 4 Å for transmission) this method has not been very widely used, except for surface observations of wear damage, fatigue and for studies of surface films, e.g., after corrosion (see Refs. 43, 44, 46, 47). Figure 17 is an example of a reflection electron micrograph showing extrusions from a fatigued aluminum crystal.

There are many complex interactions which occur when electrons travel through crystals. The most important of these is diffraction since this is the major phenomenon giving rise to contrast in the image.[49] The interpretation of contrast phenomena thus depends entirely on the theory of diffraction.[49-52] This theory has now been developed to account for unusual effects associated with absorption and provides extremely useful

and detailed information.[52] Because of the small wavelength of electrons the diffraction angles are very small ($\sim 10^{-2}$ rad.) so that only planes which are approximately normal to the foil surface will diffract. It should also be remembered that the image is a projection of the crystal so that geometrical factors must be allowed for when the images are being interpreted.

In order to accomplish direct lattice resolution, the transmitted and diffracted beams must combine at the image plane. Hence, the angle 2θ between these beams (Fig. 13) must be less than the effective aperture of the objective lens. In order to minimize aberrations the lens aperture α_o is $\sim 10^{-2}$ radian. Hence the resolution limit is $\sim \lambda/2\,\alpha_o$. For 100 kV electrons $\lambda = 0.037$ Å, hence the minimum resolvable spacing is just below 4 Å. For this reason lattice planes in metals cannot be directly resolved, although planes have been resolved in pthalocyanine and MoO_3 crystals. Figure 18 is an example of 12 Å resolution. Indirect resolution is possible by means of moiré images.[53]

With metallurgical specimens, contrast is obtained by not allowing the diffracted beams to contribute to the image. This is accomplished by the use of 30μ apertures in the back focal plane of the objective lens (Fig. 13), and a bright field image is thus formed. The dark field image is obtained by allowing a single diffracted beam to reach the image plane. With the facilities for selected area diffraction, detailed information regarding substructure can be obtained and the dark field technique is an invaluable aid in indentifying microstructural features. Figure 19 is an example of bright and dark field images of mechanical twins observed in explosively deformed copper.

The transmission technique is very powerful for investigations of lattice defects (for reviews see, e.g., Refs. 39, 48, 54): A defect producing a displacement $\vec{R}$ causes a change in phase of the diffracted beam so that phase contrast is obtained in the image.

As can be seen from Bragg's Law illustrated in Fig. 20, when $\vec{R}$ lies in the reflecting plane, the path (or phase) difference is the same as for a perfect crystal. Since the reciprocal lattice vector $\vec{g}$ is perpendicular to the reflecting plane the condition for invisibility is $\vec{g}\cdot\vec{R} = 0$.[49] As discussed earlier with regard to x-ray images (Section 3) several reflections must be studied in order to evaluate $\vec{R}$. Similar rules apply to lattice strains arising from coherent precipitates in alloys (e.g., Guinier-Preston zones).[48]

Figure 21 shows dislocations formed in silicon after a diffusion treatment. In (a) the 040 reflection operates and both sets of dislocations are visible. After tilting the specimen so that the 220 reflection operates (b) one set disappears, hence the invisible set must thus have the Burgers vector a/2 [1$\bar{1}$0] and they are edge dislocations.

Defects lying on an inclined plane give rise to oscilliatory images due to dynamical interactions between the transmitted and diffracted beams. Typically, stacking faults, twin boundaries, grain boundaries, thin precipitates all show extinction fringes (Fig. 22). The extinction distance[49-52] depends upon the operating reflection and the wavelength of electrons and some values are given in Table II. These values are several orders of magnitude smaller than the corresponding x-ray extinction distances.

Besides being able to determine the direction of the displacement vector $\vec{R}$ it is also possible to find its sign.[49-52] Thus positive and negative dislocations, intrinsic and extrinsic stacking faults, vacancy

Table 2

Extinction distances t_o for low order reflections (two beam case), λ=0.037Å

Metal	Z	t_o (1) in Å		
BCC		110	200	211
V	23	370	540	710
αFe	26	295	445	590
Mo	42	260	385	465
W	74	180	250	310
FCC		111	200	220
Al	13	640	770	1240
Ir	77	170	190	270
hcp		00.2	01.1	01.0
Mg	12	935	1155	1770
Zn	30	380	500	785

(1) These values are obtained from scattering factors based on the rest mass of the electron and are not corrected for relativity. Consequently, they are about 10% too large.

and interstitial loops and tensile or compressive strain fields from coherent precipitates can be distinguished (for review see Ref. 55).

The thin film technique can be applied to all phases of metallography, and consequently a very large amount of information concerning substructure is being accumulated.[48] The importance of stacking fault energy as a parameter determining the arrangement of dislocations in deformed crystals has been amply demonstrated since the initial, important work of Whelan[56] (see Fig. 23). Stacking fault energy and ordering have been shown to be important with regard to transgranular stress corrosion.[57, 58] One of the great advantages of the thin film technique is that the stacking fault energy can be estimated directly from the radius of curvature R of extended dislocation nodes,[56] by using the relation

$$\gamma = Gb^2/2R$$

where G = shear modulus, and b = Burgers vector of the partials at the node. Figure 24 is an example of extended nodes in α-brass from which γ is estimated to be ~ 2ergs/cm^2. The morphology and type of precipitates and dislocation-precipitate-interactions and their relation to alloy strength can be directly observed and have been extensively studied (Fig. 25). Direct observations of dislocation glide,[59] climb,[60, 61] and precipitation[62, 63] have been carried out, and the complex structures of martensites both in ferrous and non-ferrous alloys have been studied.[64, 65] Much work has been done on ordered alloys[66] and on magnetic materials.[47] The presence of magnetic or electrostatic fields in certain materials leads to refraction of the incident electrons by the specimen itself. In the case of a ferromagnetic specimen, the electron beam is split across a domain boundary and the intensity at the boundary depends on whether the

deflected electrons diverge or converge. Domain boundaries are thus alternately dark and light as shown in Fig. 26.

From this brief account it can be seen that the transmission electron microscopy technique is an invaluable tool for almost all phases of physical metallurgy.

7. Electron Probe Microanalysis

Whilst microscopy and diffraction yield information regarding size, shape, morphology and atomic arrangement they do not provide information regarding the kind and concentration of elements that may be present in a specimen. With the rapid development and use of the electron probe (originally devised by Castaing[67]) a range of elements from Z = 12 to Z = 92 (Mg-U) can be identified and quantitatively determined as well as their position to be found metallographically. A number of reviews and conference proceedings describe many applications of the probe technique.[14,15] (Also Refs. 68-70).

The incident electron beam is produced from a tungsten filament with a consider system so as to obtain a fine focus beam of diameter about 1μ. The illumination system is identical to that used in convential double condenser lens electron microscopes. As a result of electron irradiation x-rays are emitted from the sample and these can be analyzed for characteristic radiations so that individual elements can be identified. A number of probes are now manufactured commerically and are being used in many industrial research laboratories.

The principle of the method is illustrated in Fig. 27. If thin specimens are used some electrons are transmitted so that the lower part of the instrument can be used as a transmission electron microscope.

The characteristic x-ray intensity emitted from the sample is a maximum at ~90° to the incident beam, so this radiation is collected to a spectrometer 10-20° above the specimen surface. The back scattered electrons are detected by a phosphor followed by a photomultiplier. If deflecting coils are used to scan the incident beam over the object an image of the object is obtained with a resolution of ~1μ. Both the electron images and x-ray images can be displayed on cathode ray oscilloscopes just as for television. An optical microscope enables the specimen to be viewed by the operator during scanning. After each scan a characteristic contamination spot is formed where the beam strikes the surface. These spots are useful for identifying the areas examined (Fig. 30a). By selecting various characteristic wavelengths of the elements in the material their location in the specimen is readily detected. For example, in Fig. 28 taken from an Al-30%Ag alloy the x-ray image of the AgK_α emission is shown together with the intensity trace after scanning across the boundary. The depletion of Ag on opposite sides of the boundary is quite obvious. Figure 29 is a similar picutre but taken with the reflected electrons. The AgK_α intensity trace is superimposed, illustrating again the depletion of silver adjacent to the grain boundary.

It is important to prepare flat surfaces, because hills or valley will erroneously indicate enhanced or depleted material. In practice polishing with 1μ diamond is satisfactory. Surface films can be a nuisance so cleanliness is essential. If intensities are to be measured it is important to set up a system of standards all of which are treated in identical fashion to the material being investigated. The absolute magnitude of the concentration of an element is difficult to measure because of uncertainties associated with absorption processes.

It can be seen that the probe technique is extremely valuable for studies of precipitation, diffusion, segregation, inclusions, corrosion, etc. Figure 30 is an example of a diffusion experiment. In (a) the graphite region is at the far left. The area of the reaction zone traversed by the electron microprobe for x-ray spectral analysis is identified by the characteristic contamination traces. X-ray analysis showed that the layers adjacent to the graphite and tungsten to be ZrC (88 wt. % Zr) and W_2Zr (23 wt. % Zr) respectively, as a result of the diffusion reaction. The central region is a mixture of large W_2Zr grains in matrix of 96% Zr. The probe is also now widely used for mineralogical investigations. The technique has already proved to be immensely valuable in metallurgical research. It can be applied to most situations in which there are significant variations in concentration of elements over distances of microscopic order. It should also be possible to use the method for establishing phase diagrams. In ferrous metallurgy it is not yet possible to distinguish carbides from nitrides when present in small quantities.

Kossel-Lines

Since the probe provides a fine focus electron beam, a specimen can be used as a target for producing a divergent x-ray diffraction pattern. A single crystal gives a large number of light and dark lines called Kossel lines[71, 72] from which the most accurate determinations of lattice parameter can be made.[73] In order to avoid electron transmission and to produce optimum x-ray diffraction, the thickness of the specimen must be ~.004 to .01 ins. On a positive photographic print the dark Kossel lines correspond to absorption conics. Figure 31 is an example of Kossel lines.

Kossel patterns can also be obtained using a micro-focus x-ray tube. This technique can be readily combined with projection x-ray microscopy since the specimen position is the same in both methods.(14)

Besides the advantages of obtaining very accurate lattice parameter measurements and orientations the technique is a sensitive one for studying crystal perfection, e.g, from strained materials the Kossel lines are split. From measurements of the fragmentation information regarding internal strains in the material can be obtained.(14, 15)

Acknowledgements

I wish to thank those who have contributed illustrations to this paper. Their names are given in the corresponding figure captions.

This work was supported in part by the auspices of the U.S. Atomic Energy Commission.

References

1. R. Fichter, S. Arch. Wiss und Tech., 28, 235 (1962).
2. F. L. Vogel, W. A. Pfann, H. E. Corey and E. E. Thomas, Phys. Rev., 90, 489 (1953).
3. V. R. Regel, A. A. Unusovakaya and V. N. Kolomiichuk, Kristall., 4, 937 (1959).
4. W. G. Johnston, Prog. Ceram. Sci., 2, 1 (1961).
5. A. J. Forty, Adv. in Phys., 3, 1 (1954).
6. J. W. Mitchell, Direct Observations of Imperfections in Crystals, Interscience, New York, 1962, p. 3.
7. W. J. Dash, J. Appl. Phys., 27, 1193 (1956): Dislocations and Mech. Prop. of Crystals, John Wiley & Sons, New York, 1957, p. 57.
8. See, e.g., G. T. Hahn, Acta Met., 10, 727 (1962).
9. J. R. Low and R. W. Guard, Acta Met., 7, 171 (1959).
10. D. F. Stein and J. R. Low, J. Appl. Phys., 31, 362 (1960).
11. J. Washburn, Proc. Conf. Structure of Eng. Materials, Raleigh N. C., in press.
12. J. Washburn, G. K. Williamson, A. Kelly and G. W. Groves, Phil. Mag., 5, 991 (1960).
13. G. Thomas and J. Nutting, Mechanism of Phase Transformations in Metals, Inst. Metals Mon #18, 57 (1956).
14. V. E. Cosslett, Met. Reviews (Inst. Metals London), 5, 225 (1960).
15. X-Ray Microscopy and Microanalysis, Elsevier Austerdam, 1960.
16. X-Ray Microscopy and Radiography, Academic Press, New York, 1957.
17. J. J. Trillat, Met. Rev., 1, 3 (1956).
18. W. F. Berg, Z. Krist., 89, 286 (1934).

19. C. S. Barrett, Trans AIME, 161, 15 (1945).

20. A. R. Lang, J. Appl. Phys., 29, 597 (1958).

21. Direct Observations of Imperfections in Crystals, Interscience, New York, 1962.

22. S. Weissman, see Ref. 15, pp. 488, 497.

23. J. B. Newkirk, Trans. AIME, 215, 483 (1959).

24. H. Johannson, Ann. Physik, 18, 385 (1933).

25. W. G. Burgers and J. J. A. P. van Amstal, Physica, 4, 15 (1937); ibid., 5, 305 (1938).

26. G. W. Rathenall and G. Baas, Physica, 17, 117 (1951).

27. R. D. Heidenreigh, J. Appl. Phys., 26, 757, 879 (1955).

28. E. Eichen and J. W. Spretnak, Trans A.S.M., 51, 454 (1959).

29. V. Barucha, G. A. Mancini, G. W. Powell and J. W. Spretnak, Trans AIME, 221, 498 (1961).

30. E. Eichen, R. Speiser and J. W. Spretnak, WADC Tech. Report 56-328 (1956).

31. E. W. Müller, Z. Physik, 106, 541 (1937).

32. E. W. Müller, ibid., 131, 136 (1951).

33. E. W. Müller, 4th Int. Congress Electron Microscope (1958), Springer-Verlag, Berlin 1, p. 835 (1960).

34. J. F. Mulson and E. W. Müller, J. Chem. Phys., 38, 2615 (1963).

35. E. W. Müller, J. Phys. Soc. Japan, 18, (Sup II), 1, (1963).

36. D. G. Brandon, M. Wald, M. J. Southon and B. Ralph, ibid., p. 324.

37. A. H. Cottrell, J. Inst. Metals, 90, 449 (1961-62).

38. D. G. Brandon and M. Wald, Phil. Mag., 6, 1035 (1961).

39. G. Thomas, Transmission Electron Microscopy of Metals, John Wiley & Sons, New York, 1962.

40. Techniques for Electron Microscopy, Ed. D. Kay, (Blackwell's Sc. Pub. Oxford) 1961.

41. ASTM Special Technical Publications (a) #155 (1953), (b) #245 (1958), and (c) #262 (1959).

42. R. M. Fisher, J. Appl. Phys., 24, 113 (1953). See also Ref. 41 (a), p. 49.

43. Proc. 3rd Int. Conf. Electron Microscope, London (Roy. Mis. Soc.) 1956.

44. Proc. 4th Int. Conf. Electron Microscope, Berlin (Springer-Verlag) 1960.

45. Inst. Metals Rep. and Mon. series #8, 1950, Metallurgical Applications of the Electron Microscope.

46. Proc. European Congress Electron Microscopy 1960, Delft, Holland, 1961.

47. Proc. 5th Int. Conf. Electron Microscopy, Philadelphia (Academic Press) 1962.

48. Electron Microscopy and Strength of Crystals, Interscience, 1963.

49. P. B. Hirsch, A. Howie and M. J. Whelan, Phil. Trans. Roy. Soc., A 252, 499 (1962).

50. R. D. Heidenreich, J. Appl. Phys., 20, 993 (1949).

51. M. J. Whelan and P. B. Hirsch, Phil. Mag., 2, 1121, 1303 (1957).

52. A. Howie and M. J. Whelan, Proc. Roy. Soc., A 263, 217 (1961); ibid., A 267, 206 (1962).

53. J. W. Menter, Adv. In Physics, 7, 299 (1958).

54. A. Howie, Met. Reviews (Inst. Metals, London), 6, 467 (1961).

55. G. Thomas, ASM Symposium on Thin Films, in press, 1963.

56. M. J. Whelan, Proc. Roy. Soc., A 249, 114 (1958).

57. P. R. Swann, Corrosion Science, 19, 102 (1963).

58. D. L. Douglas, G. Thomas, and W. R. Roser, Proc. Int. Conf. Stress Corrossion, 1963, in press.

59. M. J. Whelan, P. B. Hirsch, R. W. Horne and W. Bollmann, Proc. Roy. Soc., A 240, 524 (1957).

60. J. Silcox and M. J. Whelan, Phil. Mag., 5, 1 (1960).

61. A. Eikum and G. Thomas, J. Phys. Soc. Japan, 18, (111), 98 (1963).

62. G. Thomas and M. J. Whelan, Phil. Mag., 6, 1103 (1961).

63. J. Hren and G. Thomas, Trans AIME, 227, 308 (1963).

64. P. M. Kelly and J. Nutting, J. Iron & Steel Inst., 197, 199 (1961); Proc. Roy. Soc., A 259, 45 (1960).

65. P. R. Swann and H. Warlimont, Acta Met., 11, 511 (1963).

66. M. J. Marcinkowski, see p. 333-440, Ref. 48.

67. R. Castaing, Adv. Electronics, 13, 317 (1960).

68. D. A. Melford and P. Duncumb, Metallurgia 205 (1960).

69. T. Mulvey, Iron and Steel Inst. Spec. Rep. # 68, (1960), p. 225.

70. B. R. Banerjee, W. D. Bingle and N. S. Blake, J. Metals, 15, 769 (1963).

71. D. R. Schwarzenberger, Phil. Mag., 4, 1242 (1959).

72. K. Lonsdale, Phil. Trans Roy. Soc., 240, 219 (1947).

73. B. H. Heise, J. Appl. Physics, 33, 938 (1962).

Figure Captions

Fig. 1. Widmanstatten's micrograph of a meteorite showing precipitation of the α phase.

Courtesy Professor R. F. Mehl.

Fig. 2. Martensite and retained austenite in Fe-28% Ni-0.45% C steel. The specimen was polished prior to compressive loading. In (a) slip markings in the austenite and deformation markings in the martensite are visible. After further polishing the slip markings have been removed but the markings in the martensite remain. These are thus due to mechanical twinning. x1500

Courtesy R. Munson and D. Schmatz Ford Scientific Laboratory.

Fig. 3. Etch pits at slip bands and individual dislocations in MgO.

Courtesy J. Washburn.

Fig. 4. Transmission electron micrograph of MgO showing that the debris left in a glide band contains many dislocation dipoles and loops.

Courtesy Phil. Mag. and Washburn et. al (Ref. 12).

Fig. 5. Schematic diagrams illustrating the experimental arrangements for x-ray diffraction micrography (a) Lang method, (b) Reflection Berg-Barrett, (c) Transmission Berg-Barrett.

Fig. 6. (a) A reconstructed LiF crystal as observed by the Berg-Barrett technique; subgrain boundaries, slip lines and grown-in dislocations are visible.

Courtesy J. B. Newkirk and Trans A.I.M.E. (Ref. 23).

(b) A light micrograph (LHS) showing the etched surface of a Fe-4% Si crystal containing sub-boundaries and etch pits at dislocations. Notice the corresponding but better resolved structure observed by x-ray micrography (RHS).

Courtesy J. B. Newkirk and Trans A.I.M.E. (Ref. 23).

Fig. 7. (a) Cross section of a thermionic emission electron microscope shown in (b).

Courtesy E. Eichen
Ford Scientific Laboratory.

Fig. 8. Sequence from a movie film showing the γ-α transformation in pure iron. Notice the twins being consumed in the γ phase.

Courtesy E. Eichen
Ford Scientific Laboratory.

Fig. 9. Schematic section of the field-ion microscope.

Courtesy E. W. Müller.

Fig. 10. Showing numerous surface vacancies due to corrosion of platinum surface probably caused by N_2 (see Ref. 33). The central disc is (001).

Courtesy E. W. Müller and
J. Chem. Phys. (Ref. 34).

Fig. 11. Showing interstitial damage (arrowed) in α-irradiated tungsten.

Courtesy E. W. Müller and
J. Phys. Soc. Japan (Ref. 35).

Fig. 12. Scheme showing the ray paths in a light and an electron microscope.

Fig. 13. Showing focusing action of the objective lens and the formation of the diffraction pattern and its relation to the image. Notice that directions are inverted in the image with respect to the diffraction pattern and the specimen. The bright field image is obtained by allowing only the transmitted beam A to enter the image plane.

Fig. 14. Oxide replica of an aged Al-4% Cu alloy. The white areas denote position of θ' particles. Notice array at dislocation sites.

Courtesy Inst. of Metals (Ref. 13).

Fig. 15. Carbon extraction replica (a) and (b) selected area diffraction pattern from the large chromium carbide particle in (a).

Fig. 16. Oxide replica showing slip band structure in quenched Al-Ag alloy after tensile deformation.

Fig. 17. Reflection electron micrograph showing extrusions from a fatigued specimen of aluminum.

Courtesy Inst. of Metals.

Fig. 18. Direct lattice resolution of $(20\bar{1})$ planes in copper phthalocyanine; the spacing between planes is 12.5 Å.

Fig. 19. Images of twins in explosively deformed copper:
(a) Bright field image showing two twin orientations.
(b) Diffraction pattern of (a); matrix in $[5\bar{1}0]$.
(c) Dark field image of $11\bar{1}_{T_1}$ twin spot.
(d) Dark field image of 111_{T_2} twin spot.
Notice reversal of contrast from (a) to (c) and (d).

Fig. 20. Illustrating Bragg's Law, the sphere of reflection construction in the reciprocal lattice, and the condition $\vec{g}\cdot\vec{R} = 0$. 0^*B is the reciprocal lattice vector for the reflecting planes $(hk\ell)$. When the sphere cuts through B, Bragg's Law is satisfied.

Fig. 21. Dislocation networks in silicon. Orientation [001]. In (a) the 040 reflection operates and in (b) the 220 reflection. In (b) one set is invisible.

Fig. 22. Stacking faults bounded by partial dislocations in 18/8 stainless steel. Notice characteristic extinction fringes at the faults.

Fig. 23. Showing that stacking fault energy is a factor in determining the dislocation arrangements in deformed crystals (a) nickel ($\gamma \sim 100$ ergs/cm^2), (b) stainless steel ($\gamma \sim 20$ ergs/cm^2). Notice that dislocations remain coplanar and pile-up only if the stacking fault energy is low.

Fig. 24. Showing extended nodes in Cu-33½ % Zn. The stacking fault energy is ~ 2 ergs/cm^2.

Fig. 25. Showing dislocations being held up at thoria particles in dispersion strengthened T.D. nickel.

Fig. 26. Showing magnetic domain walls in hcp cobalt. The walls lie parallel to the c-axis (arrowed).

Fig. 27. Sketch illustrating the principle of the probe microanalyzer.

Fig. 28. AgK_α x-ray image of Al-30% Ag aged 72 hours at 375°C. The Ag intensity trace across the boundary in the middle photograph is shown on the right.

Courtesy B. E.V. Clark,
Ford Scientific Laboratory.

Fig. 29. Similar to Fig. 28 but the image is of the reflected electrons. The Ag intensity trace is superimposed.

Courtesy B. E. V. Clark,
Ford Scientific Laboratory.

Fig. 30. Diffusion reaction zone of a Zr bounded W-graphite specimen. (a) optical micrograph, (b) scanned electron image of similar area shown in (a). Notice contamination spots in (a) where probe analyses were made. In (b) the diffusion zone can be clearly seen (see text for description).

Courtesy Materials Analysis Co.,
Palo Alto.

Fig. 31. Kossel line pattern of (111) single crystal of germanium. (b) Histogram of lattice parameter measurements made from the Kossel pattern.

Courtesy R. Potts, G. L. Pearson
and V. G. Macres. Stanford
University.

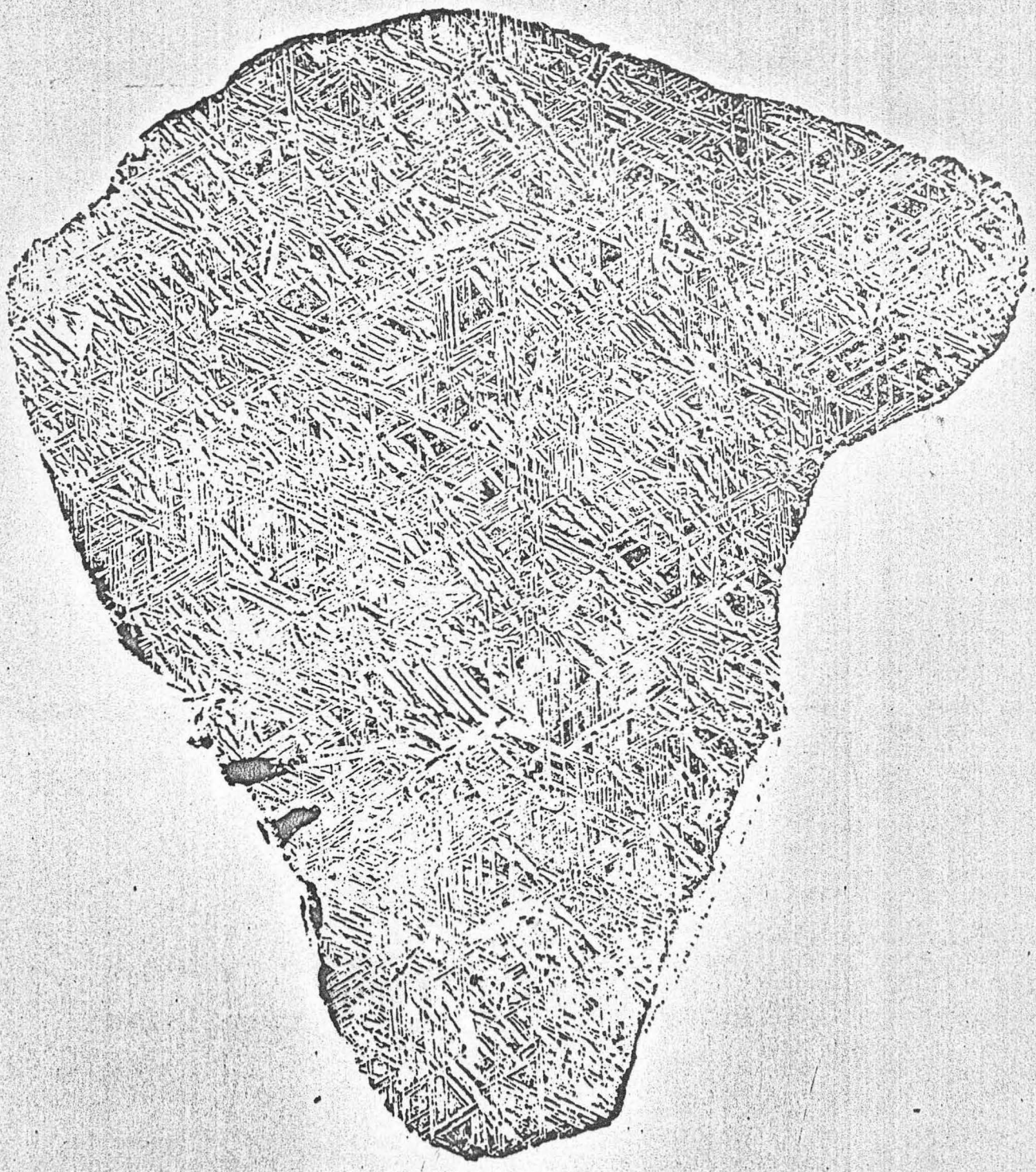

Fig. 1.

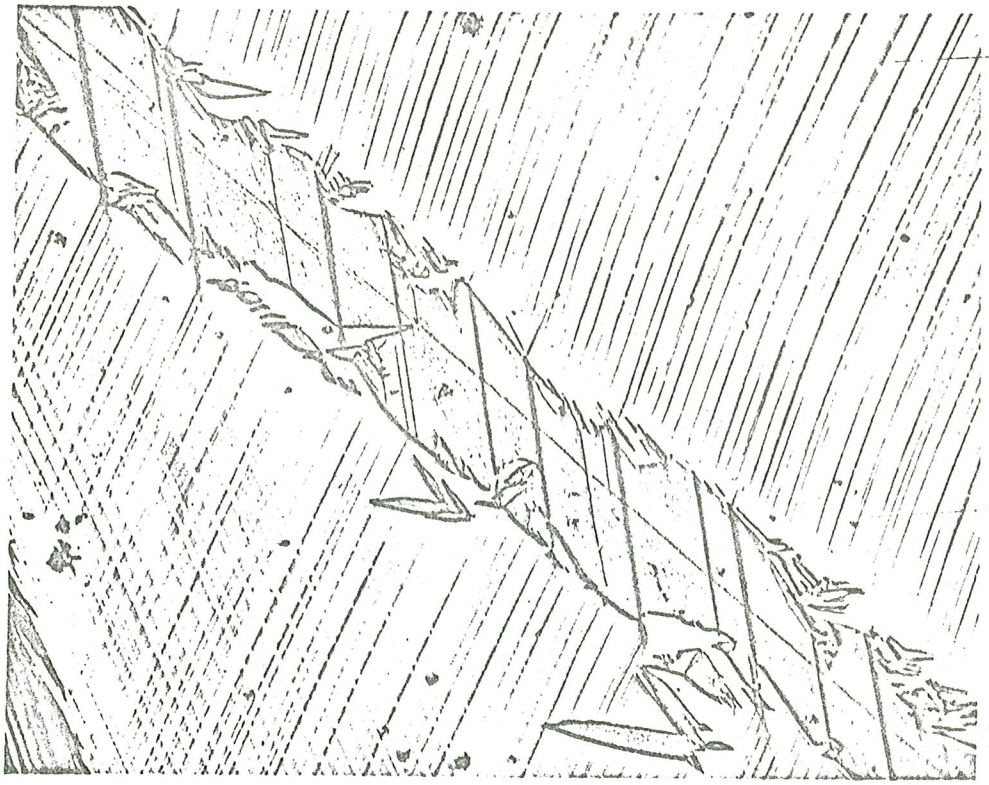

(a)

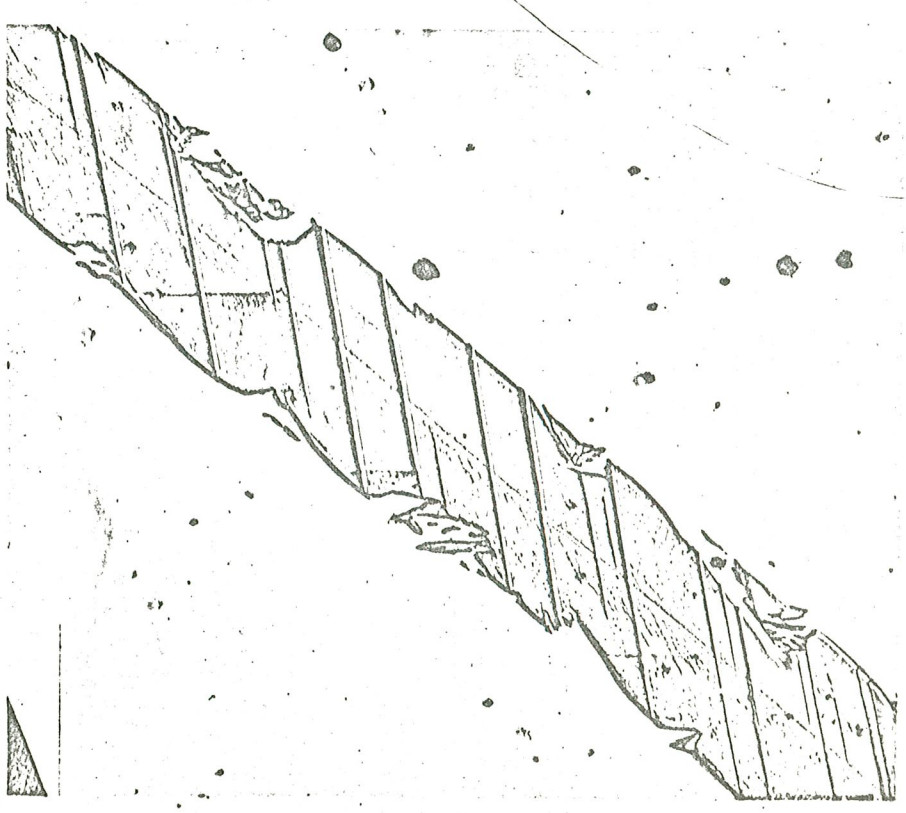

(b)

Figs. 2(a) and (b).

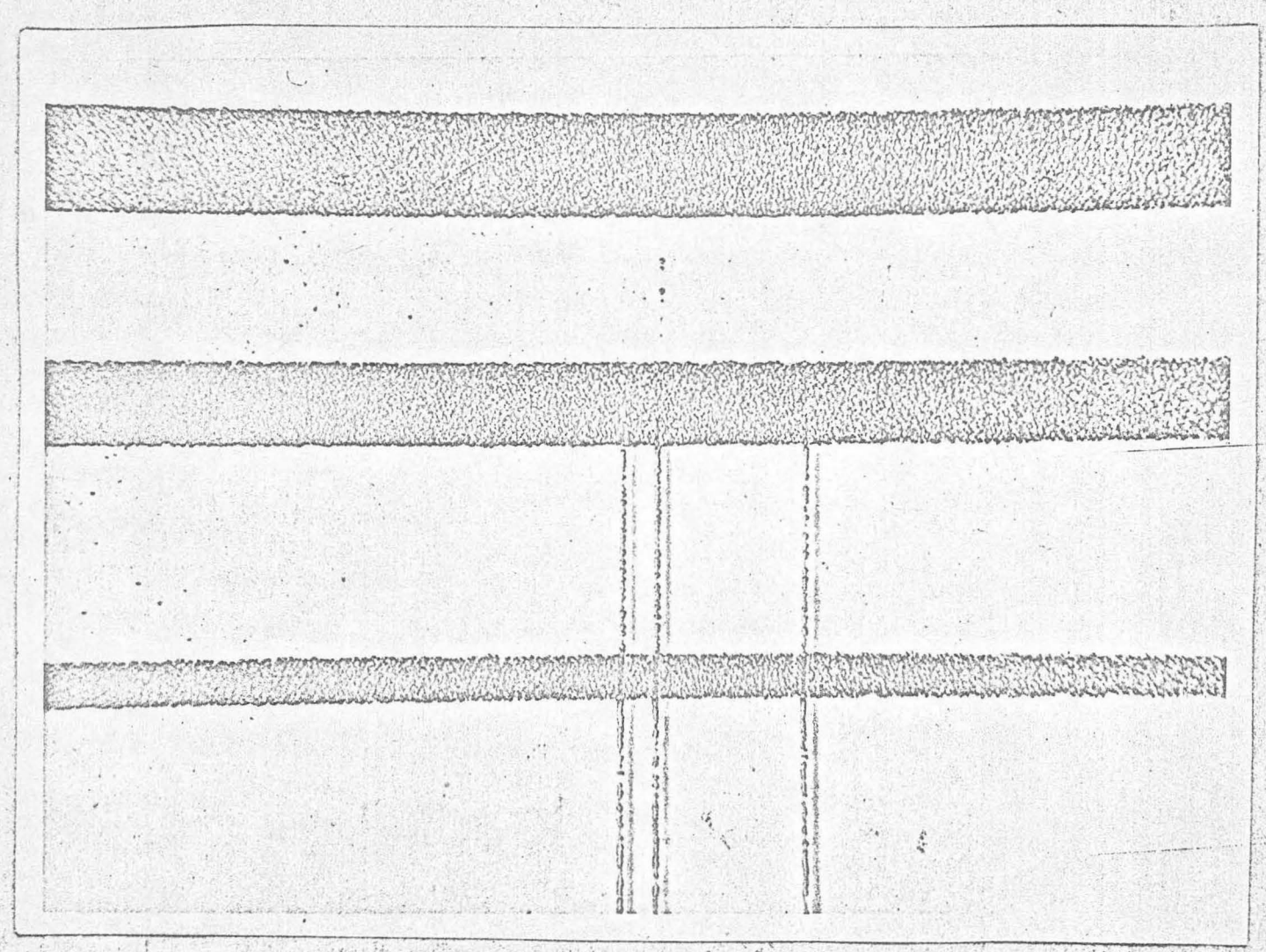

Fig. 3.

Fig. 4.

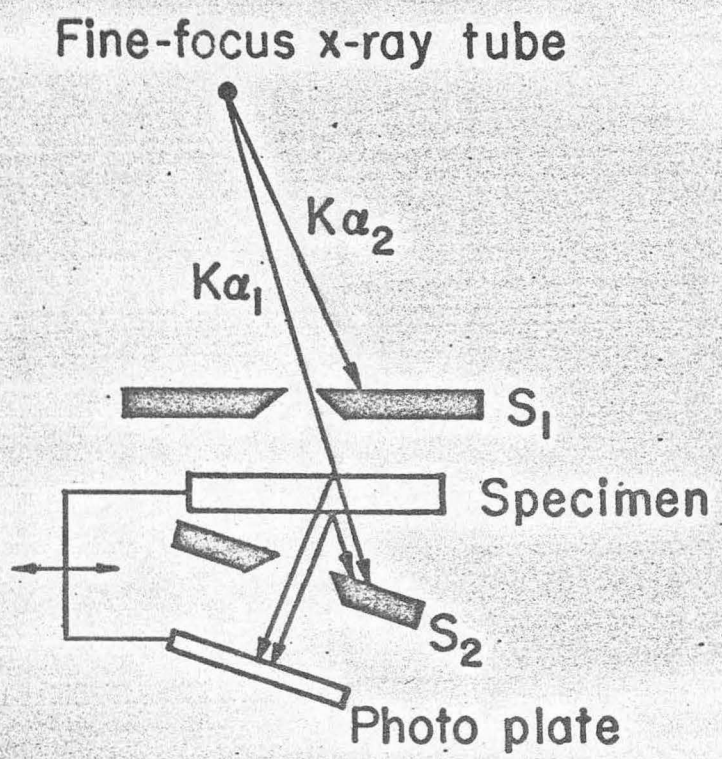

(a)

Lang method

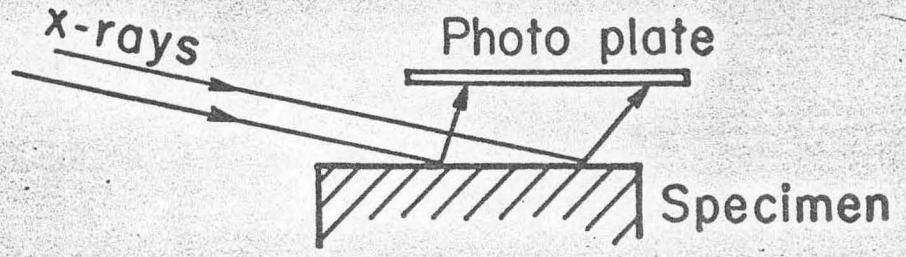

(b)

Reflection Berg-Barrett

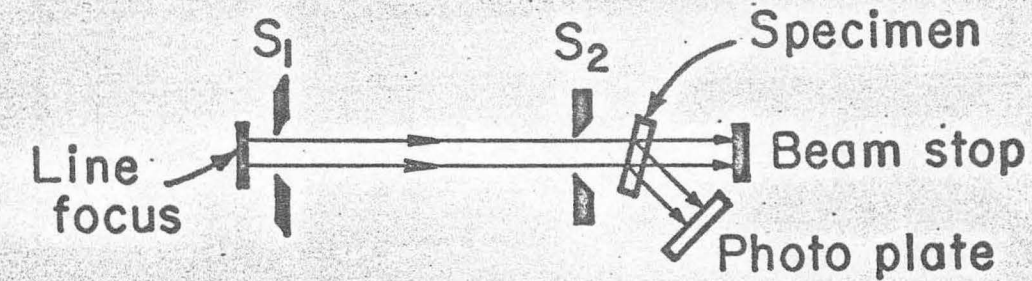

(c)

Transmission Berg-Barrett

UCRL-11067

Fig. 5.

MU-32482

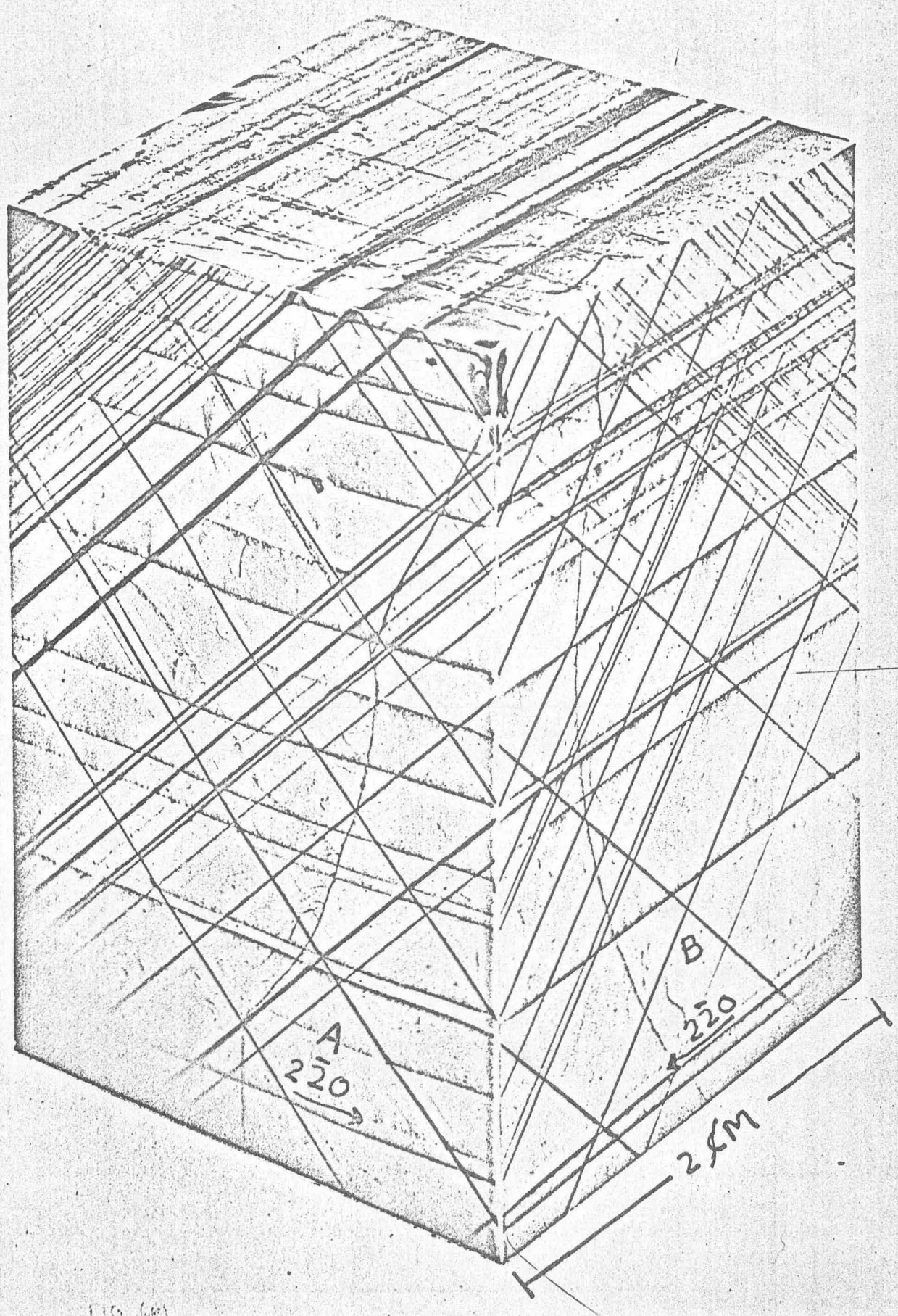

Fig. 6(a).

LHS TOP RHS

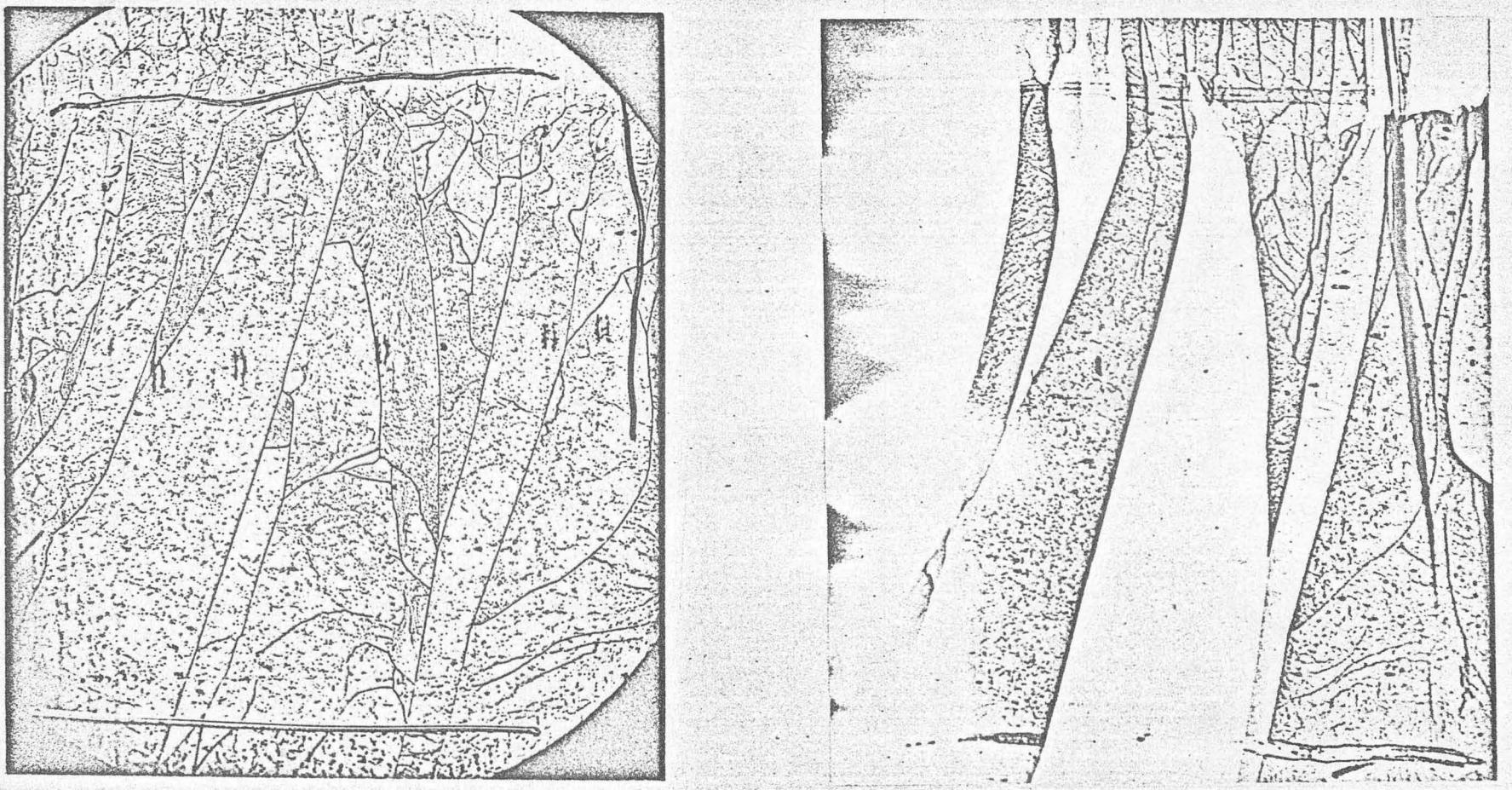

Fig. 6(b).

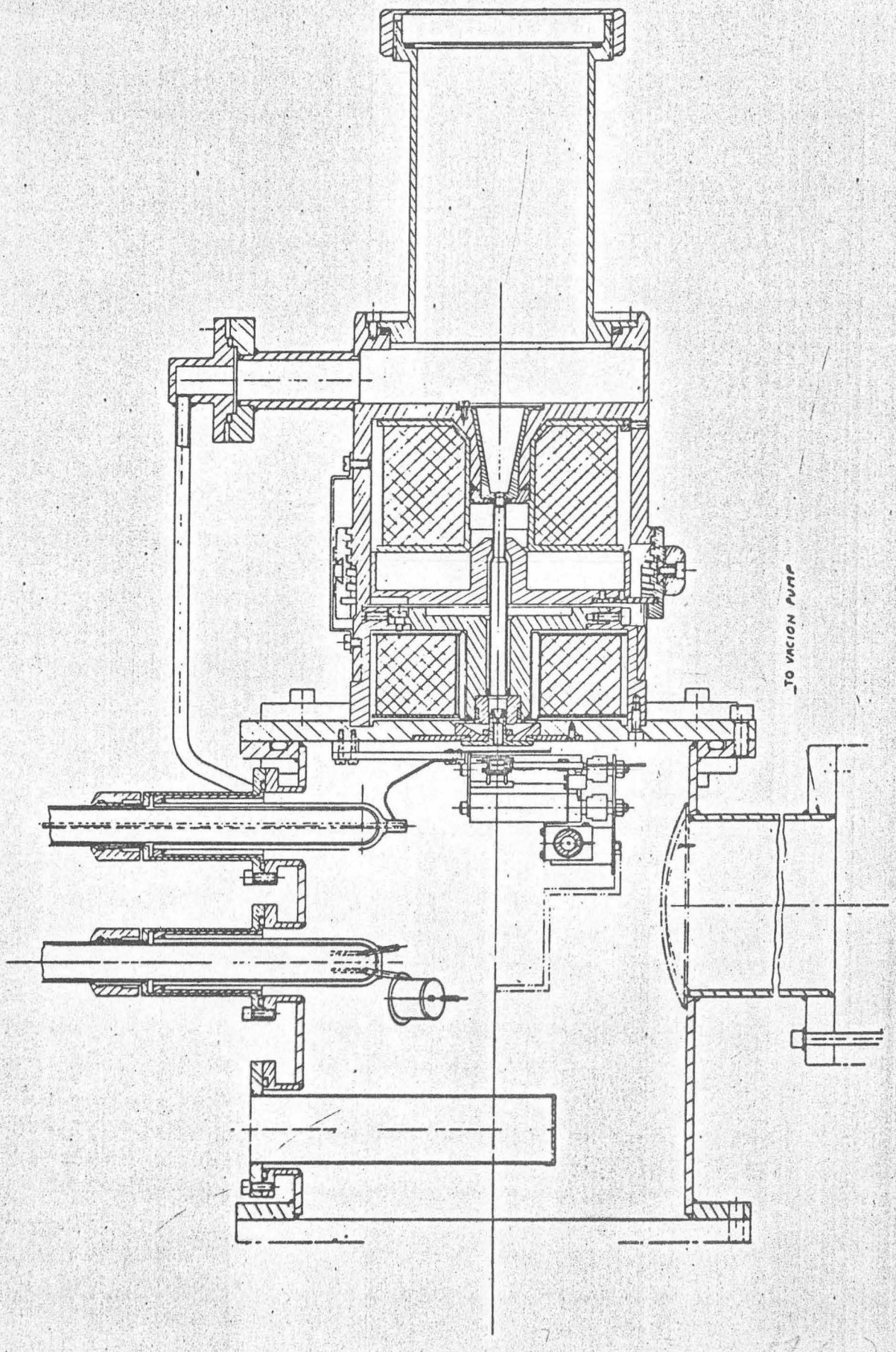

Fig. 7(a).

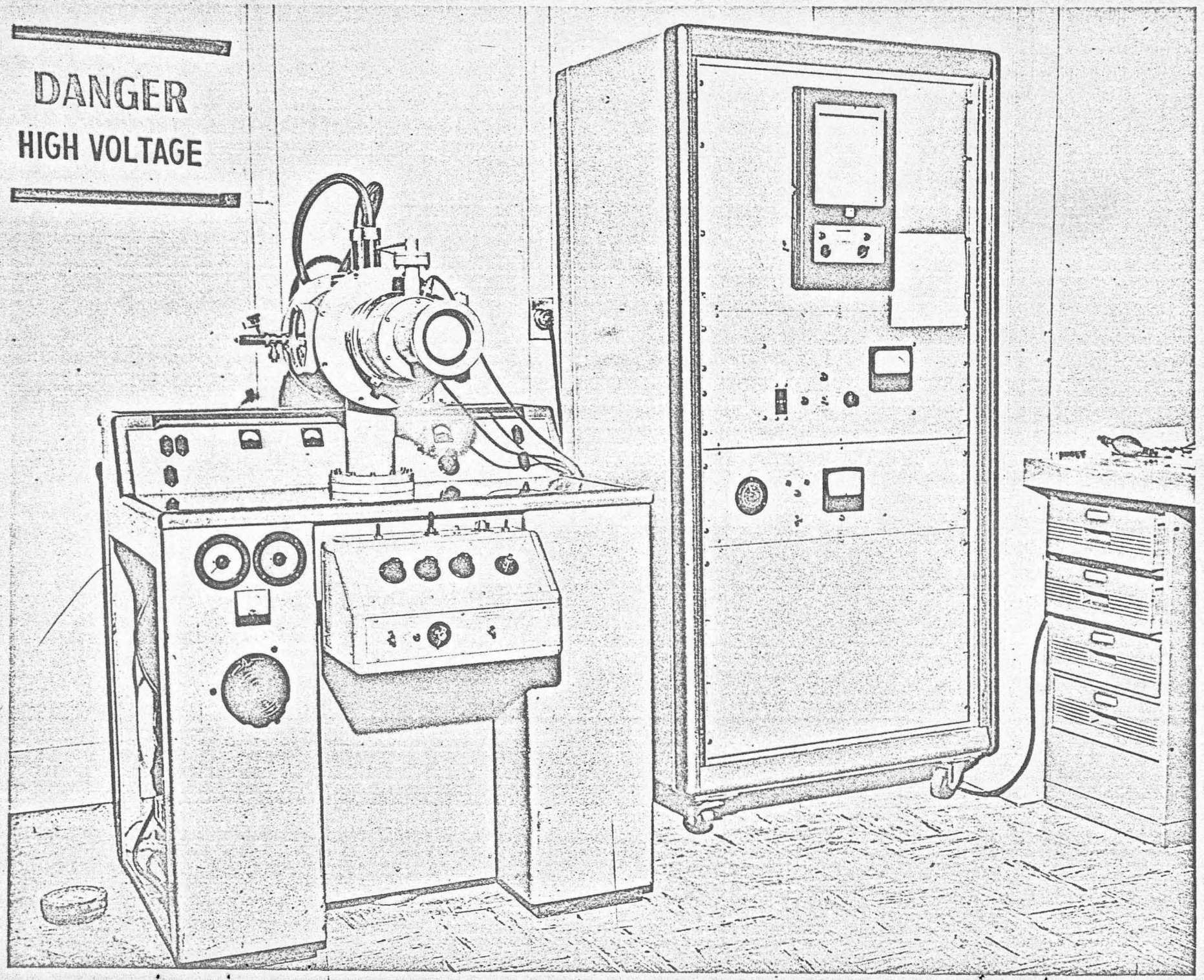

Fig. 7(b).

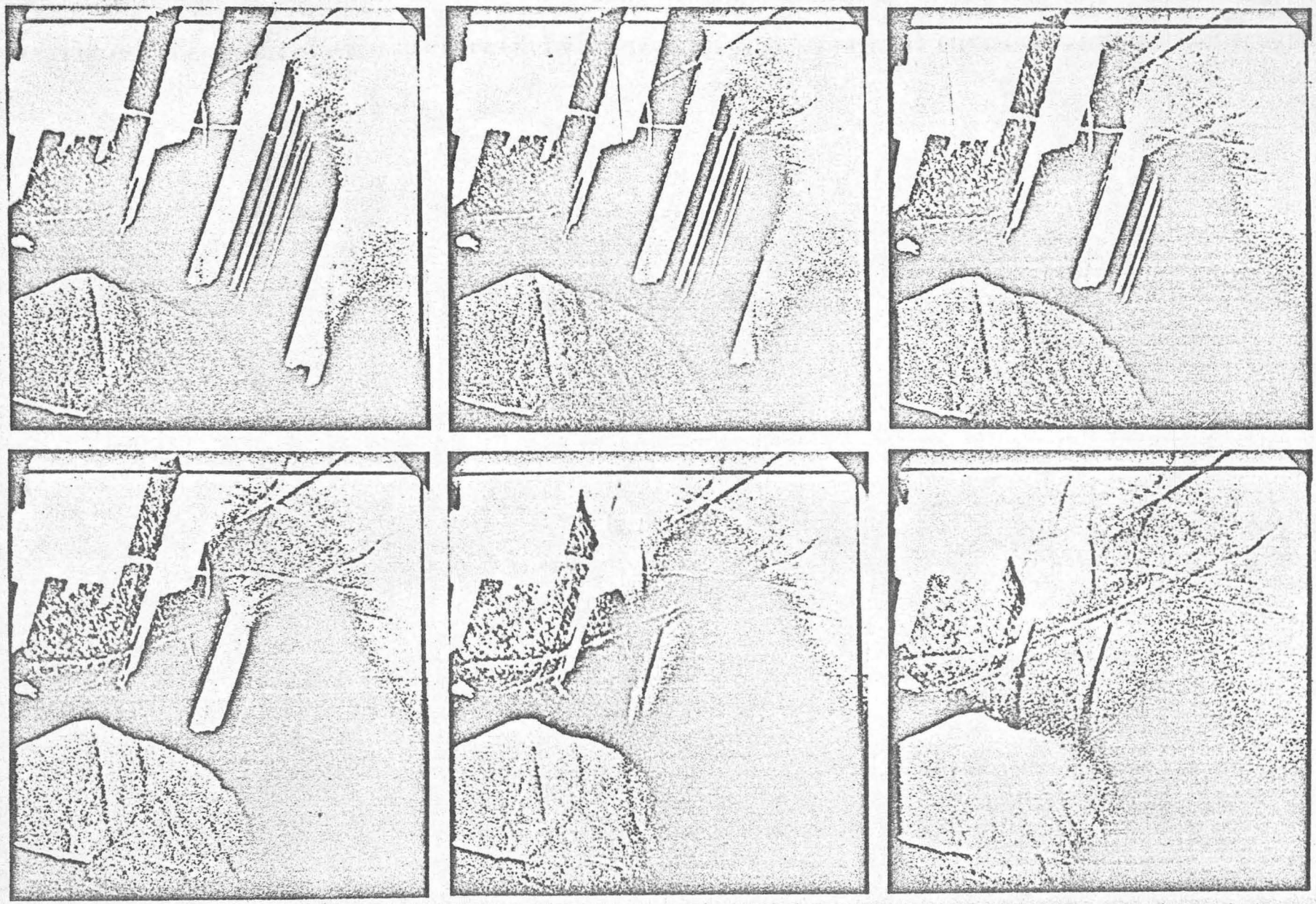

SEQUENCE SHOWING γ — α TRANSFORMATION IN HIGH PURITY IRON

(NOTE TWINS BEING CONSUMED IN γ)

Fig. 8.

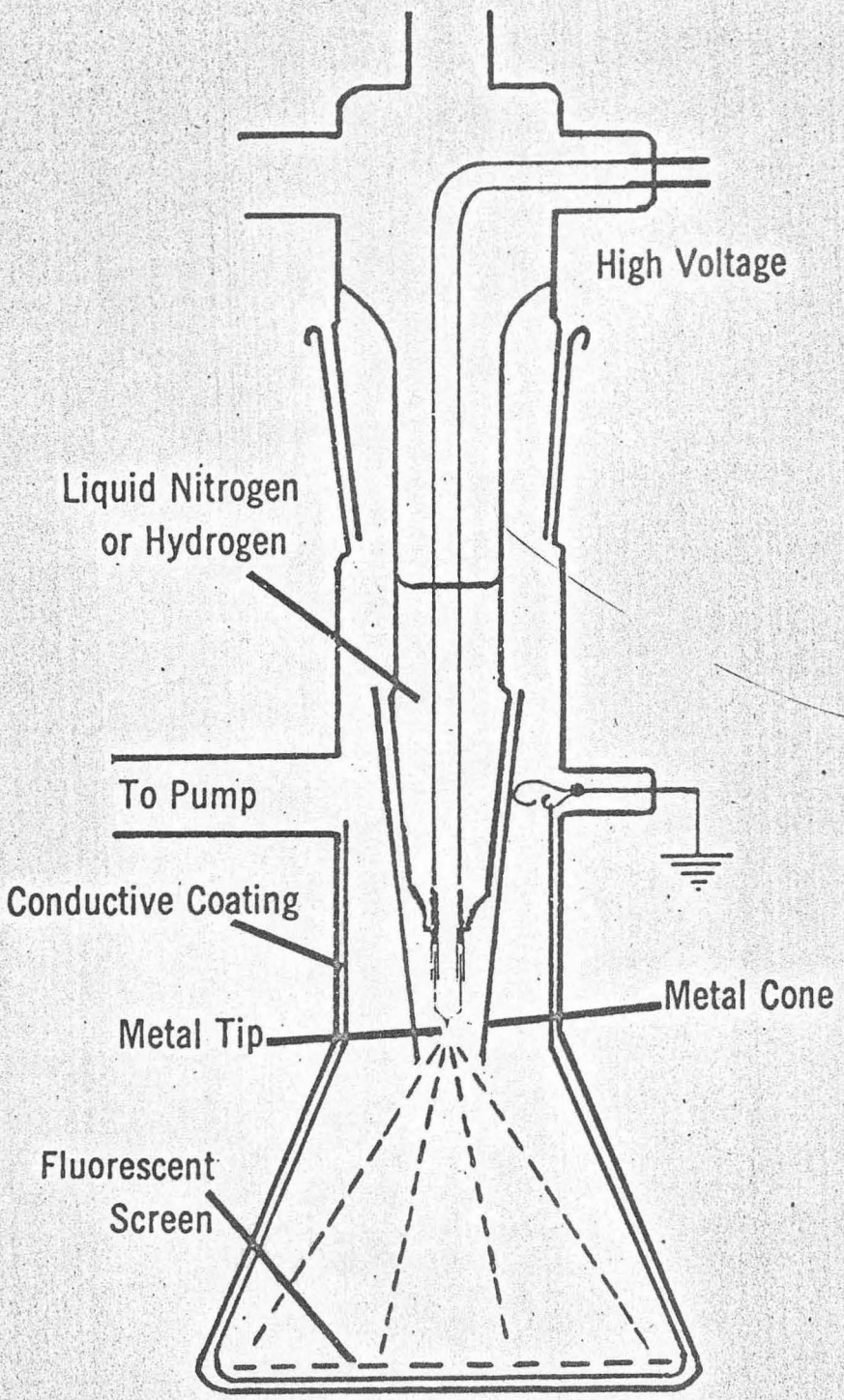
High Voltage
Liquid Nitrogen
or Hydrogen
To Pump
Conductive Coating
Metal Cone
Metal Tip
Fluorescent
Screen
MU-32254

Fig. 9.

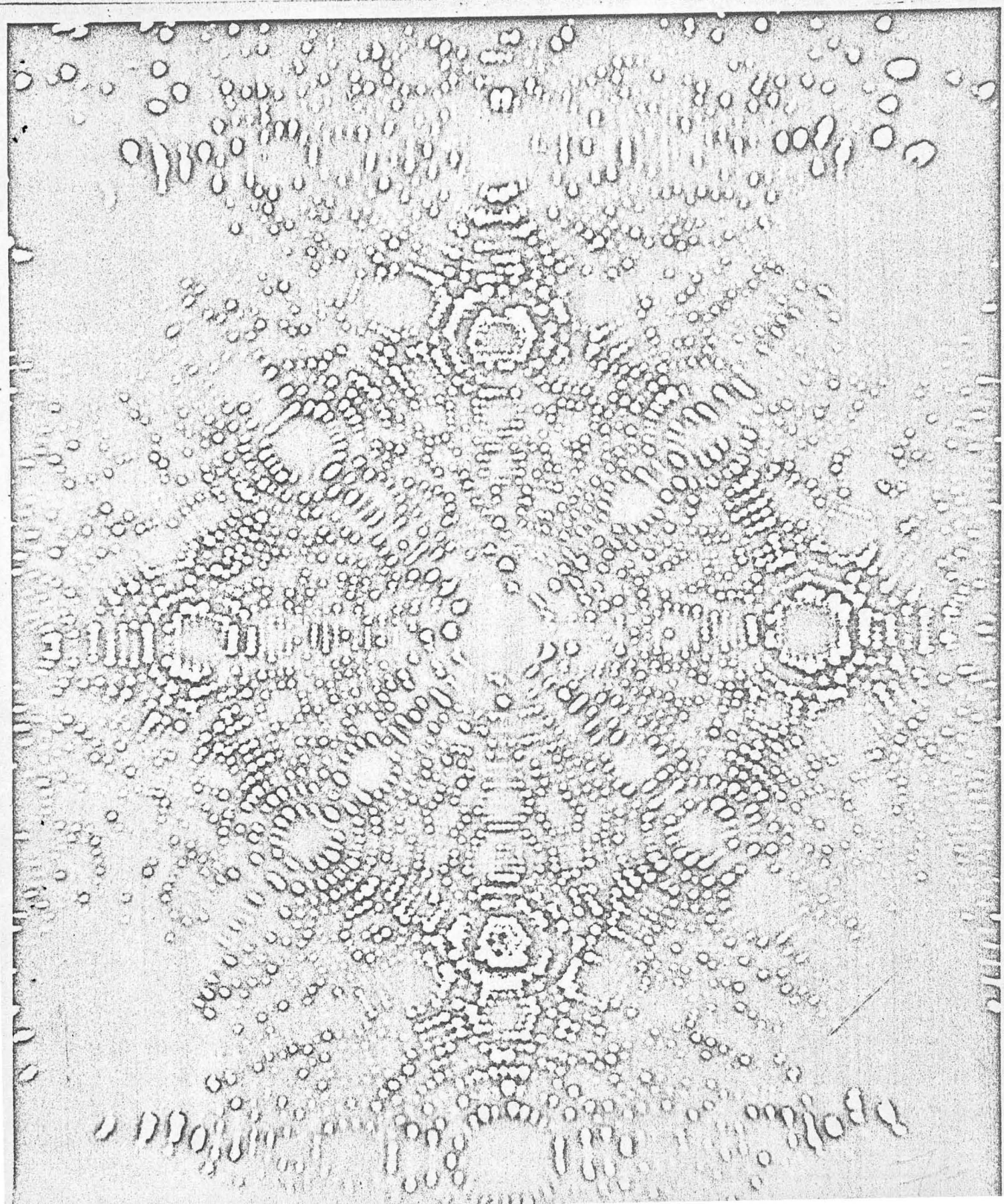

Fig. 10.

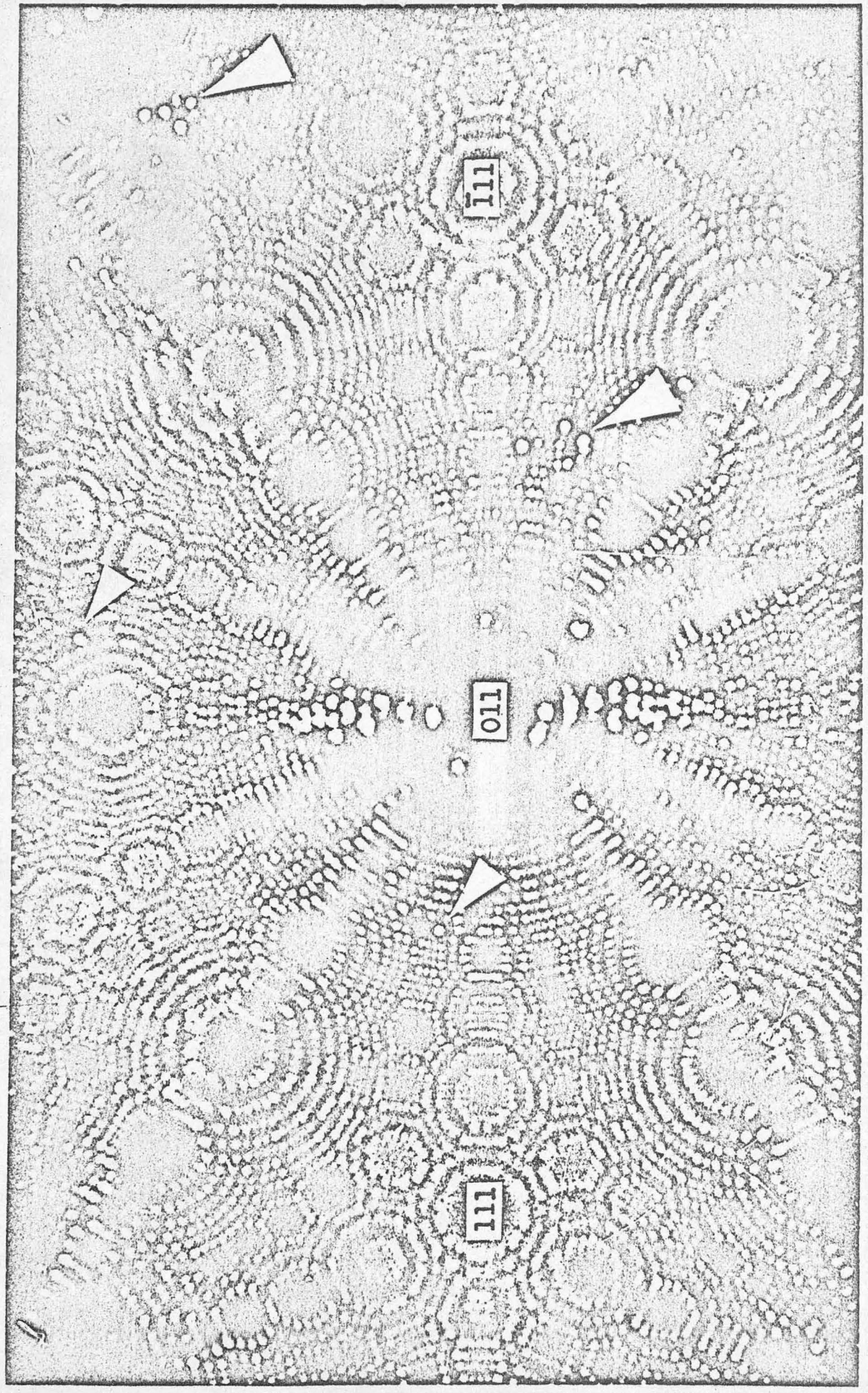

Fig. 11.

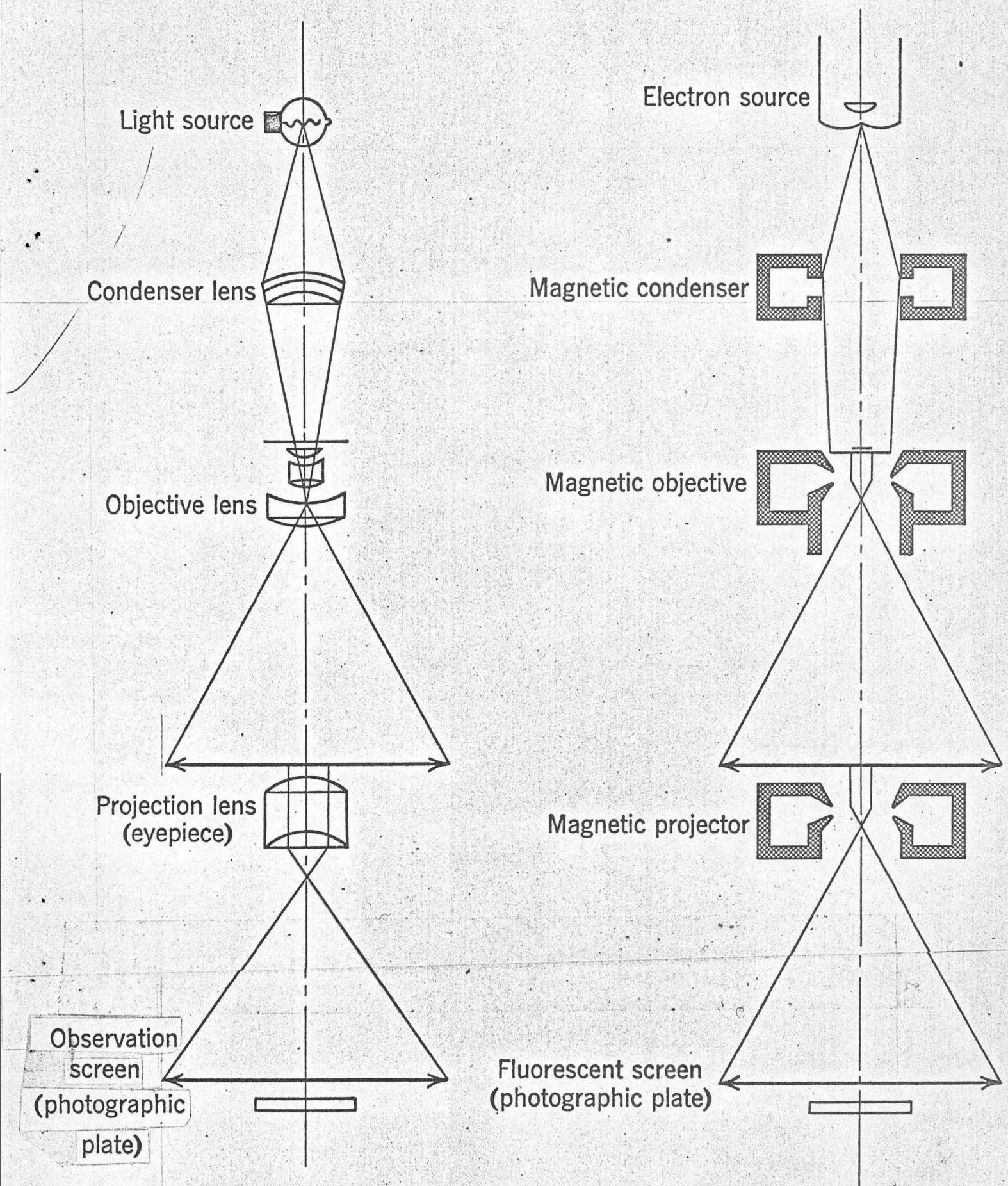
Light source
Condenser lens
Objective lens
Projection lens
(eyepiece)
Observation
screen
(photographic
plate)
Electron source
Magnetic condenser
Magnetic objective
Magnetic projector
Fluorescent screen
(photographic plate)

Fig. 12.

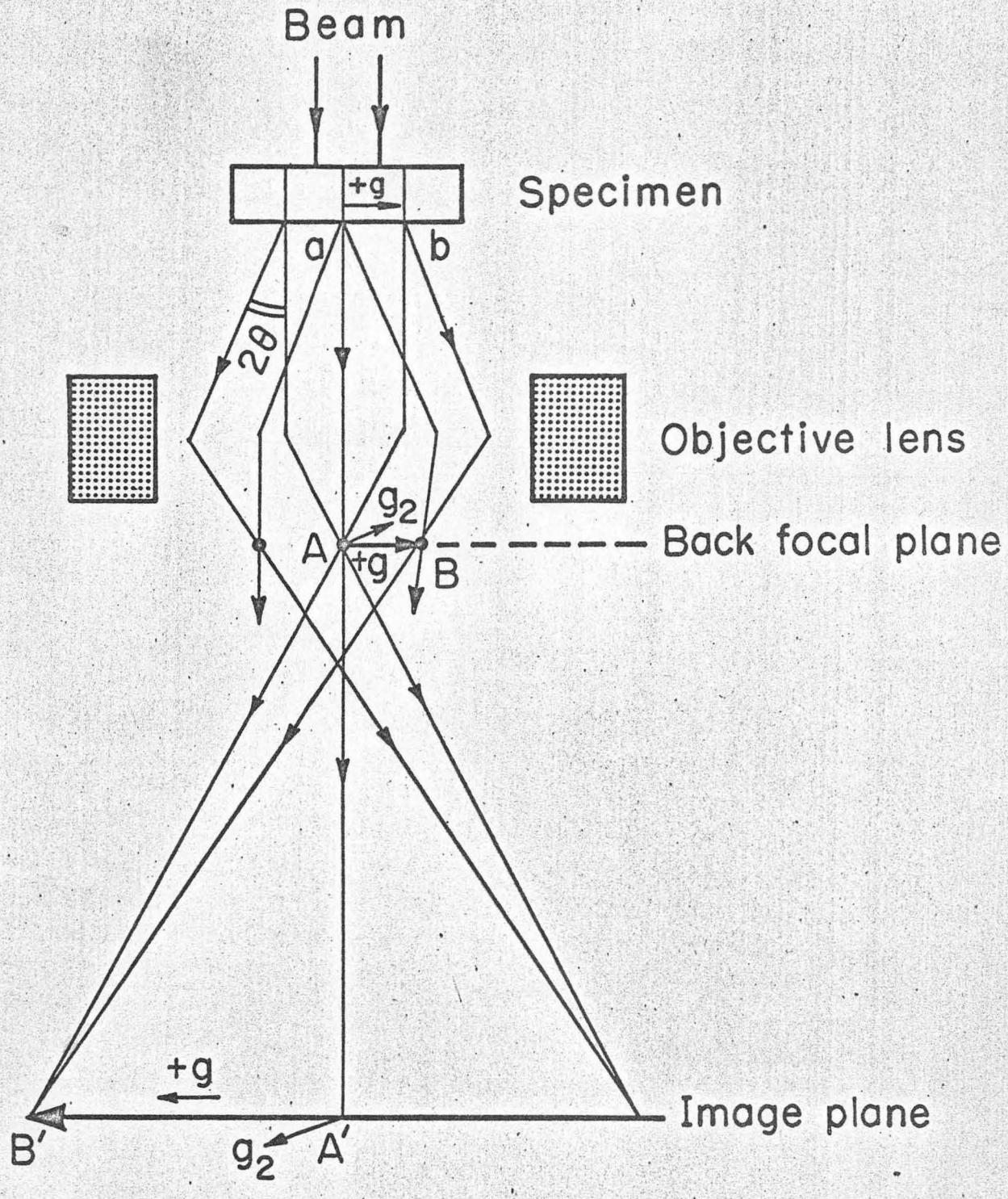
Beam
+g
Specimen
a
b
2θ
Objective lens
g2
A
+g
B
Back focal plane
+g
Image plane
B′
g2
A′
MU-32005-A

Fig. 13.

Fig. 14.

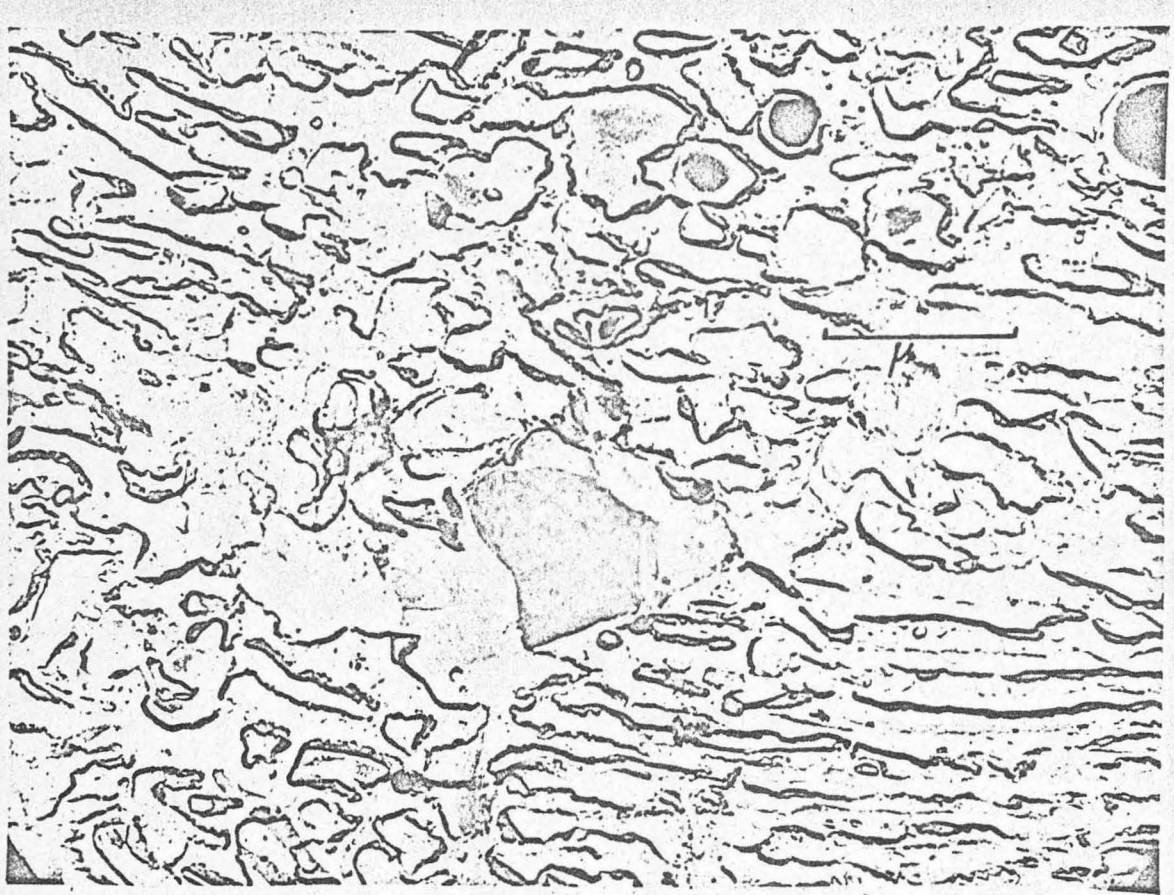

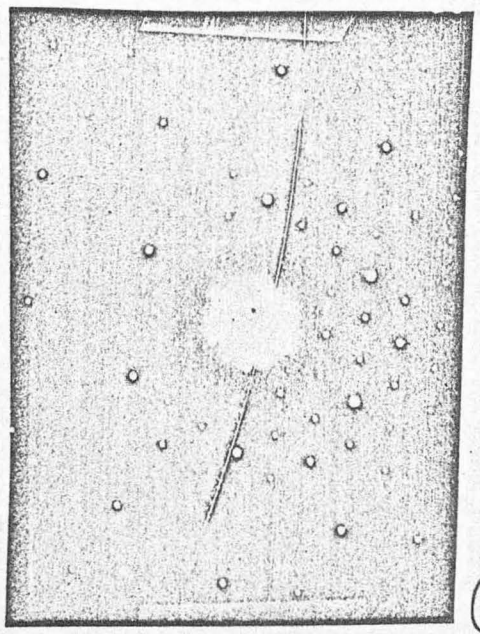

Figs. 15(a) and (b).

Fig. 16.

Fig. 17.

Top

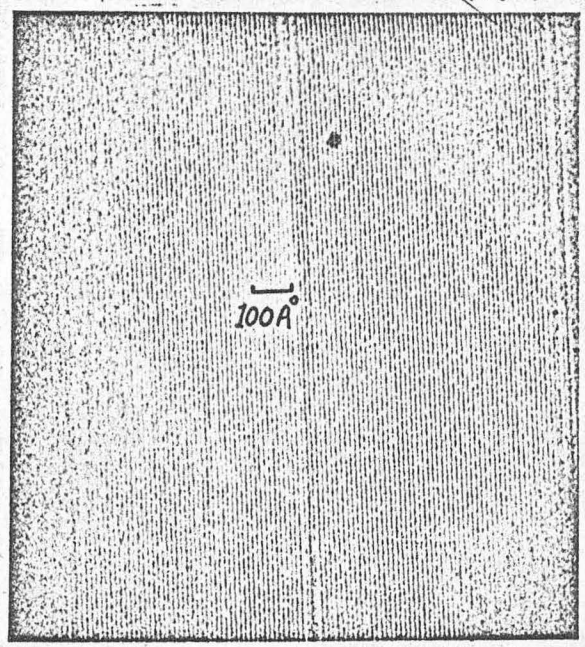

Fig. 18.

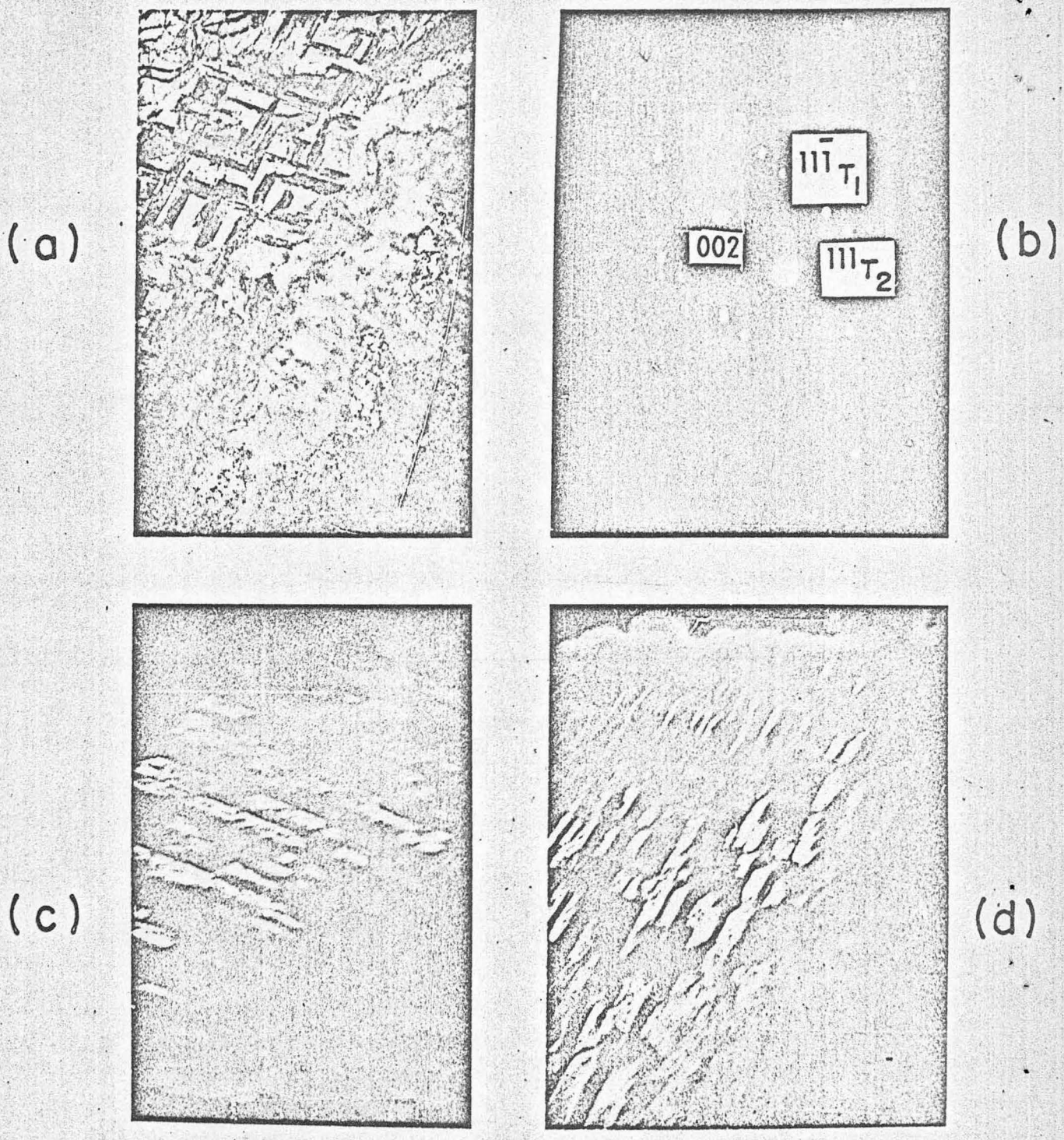

Fig. 19.

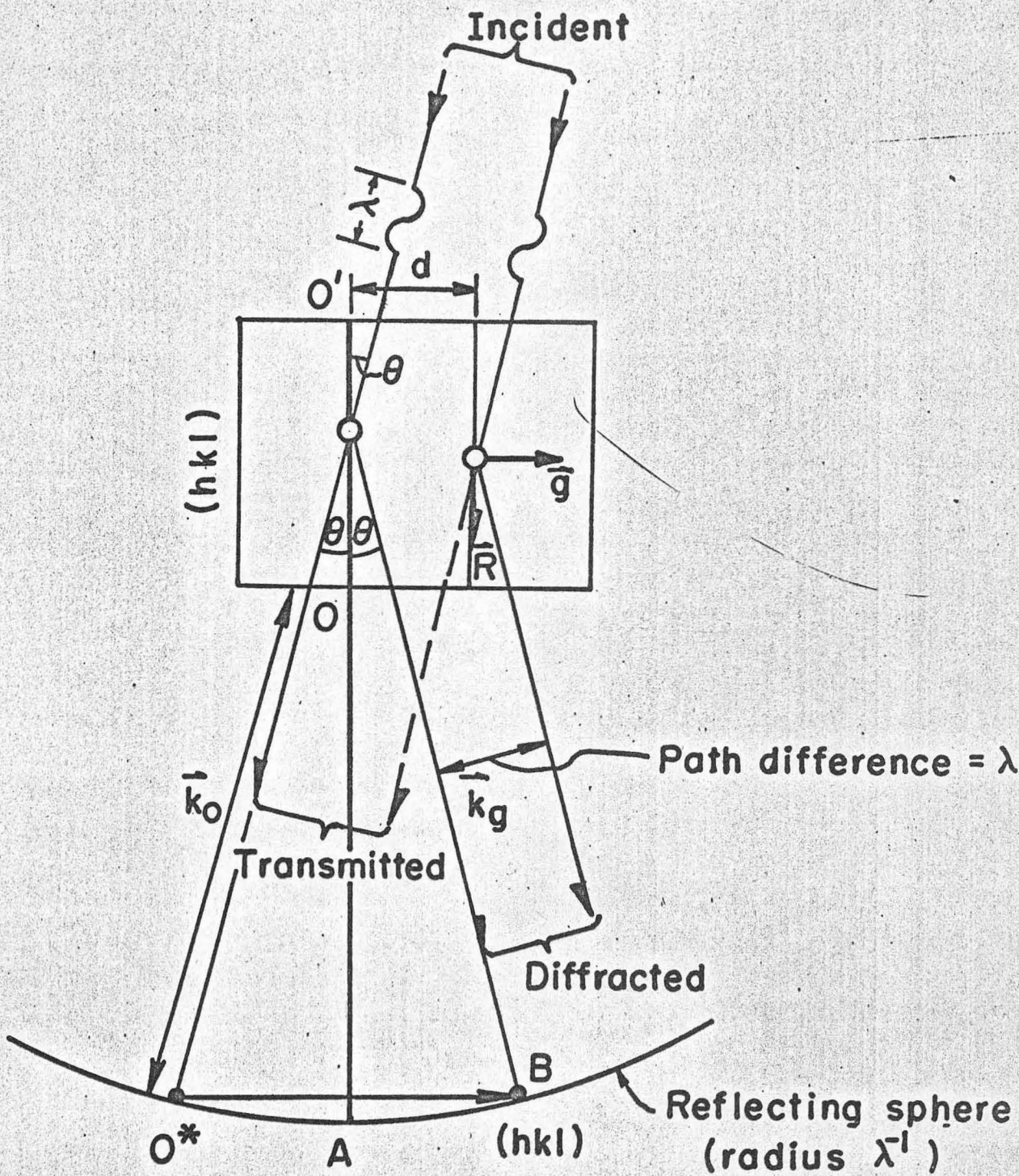

MU-32006

Fig. 20.

Fig. 2.

Fig. 21.

Fig. 22

Fig. 23(a).

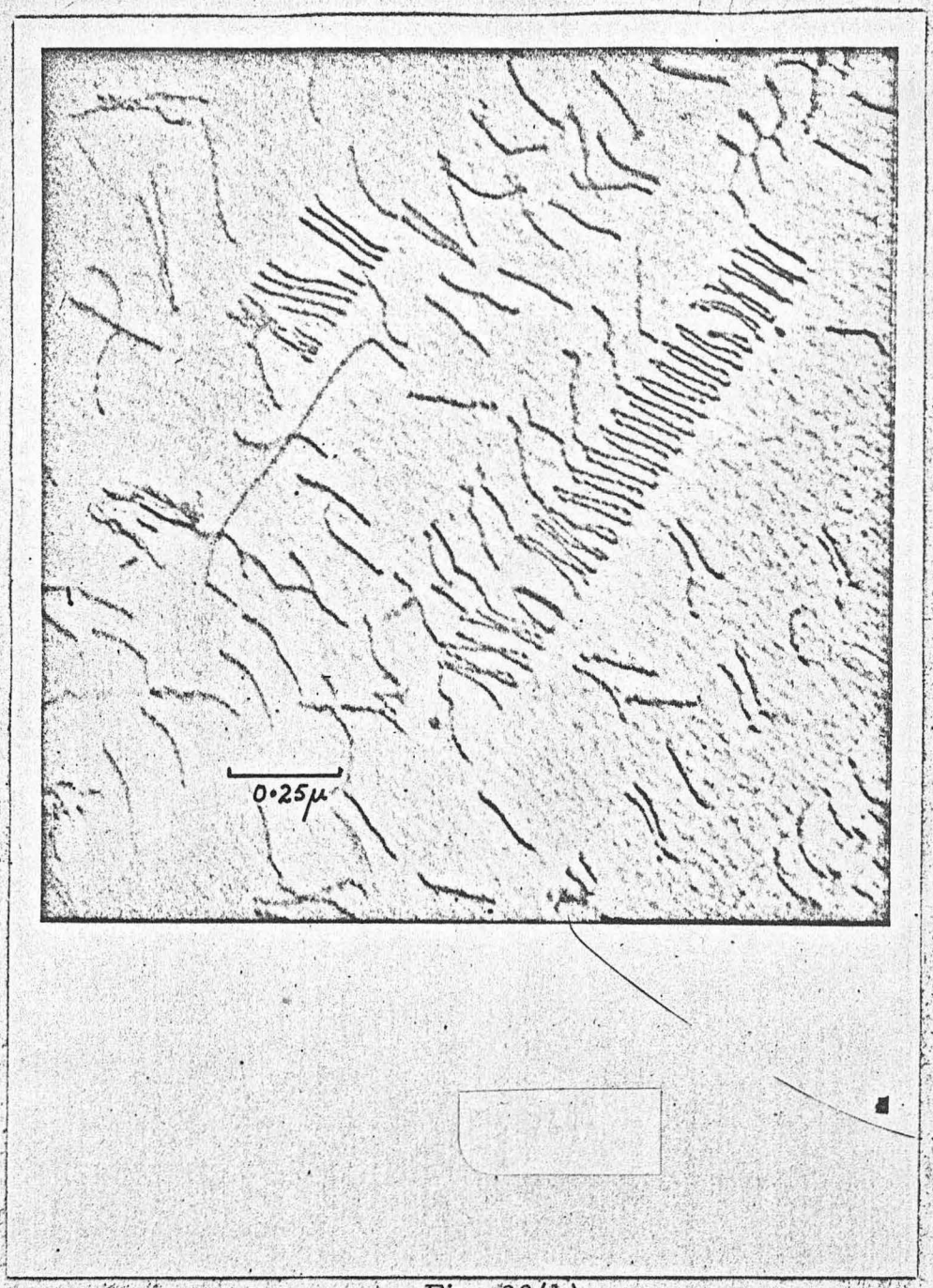

Fig. 23(b).

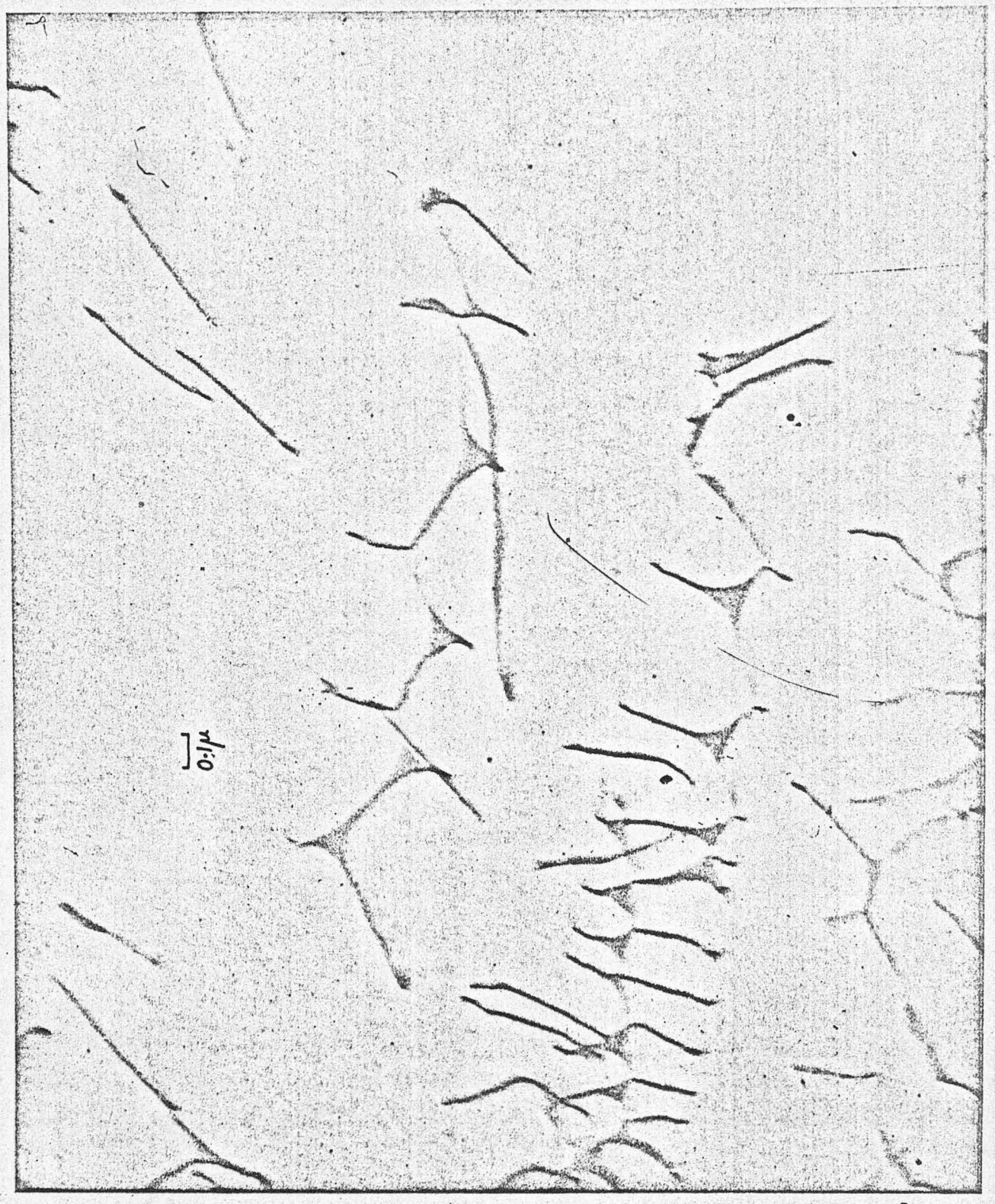

Fig. 24.

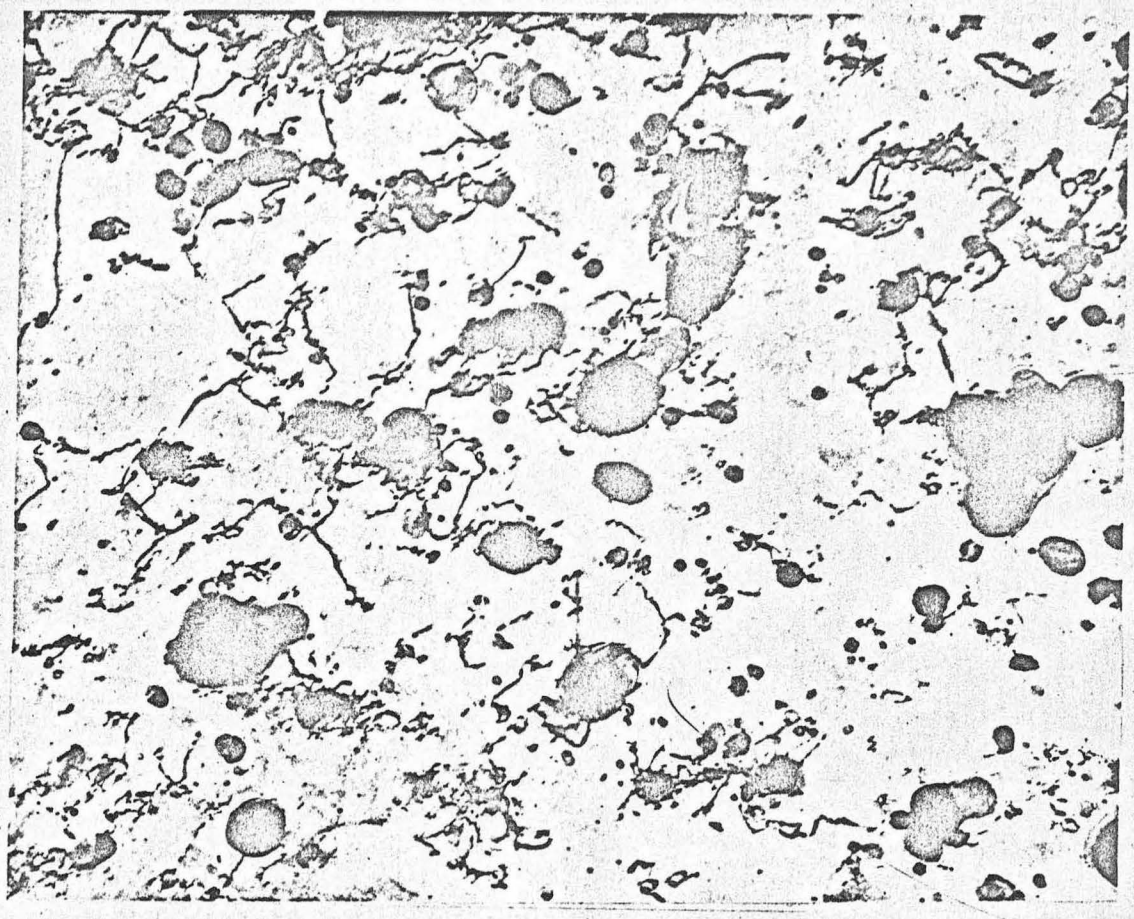

3. TD-Nickel, 900°C + 2.1% strain.

Fig. 25.

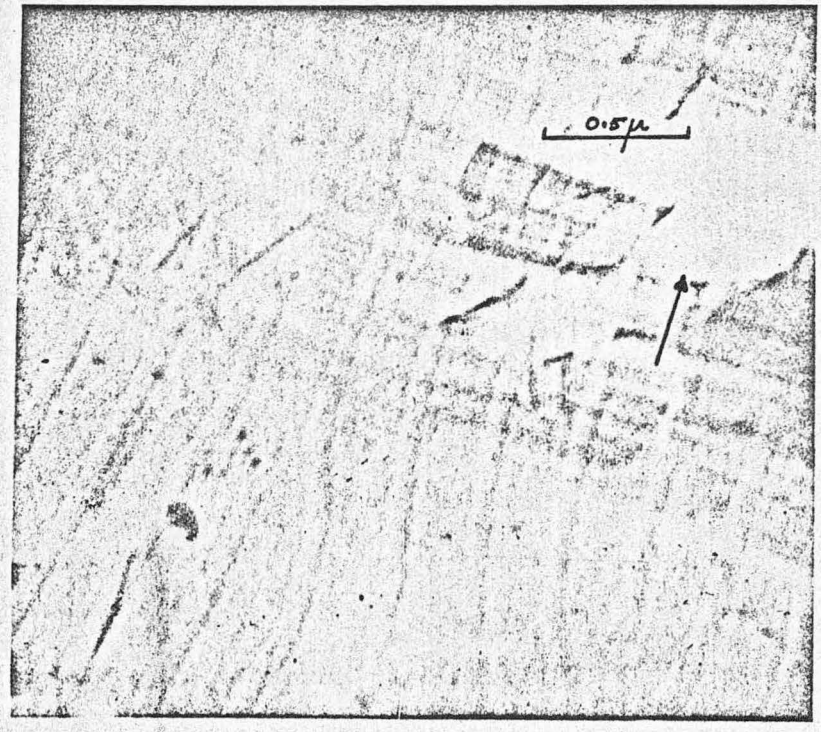

Fig. 26.

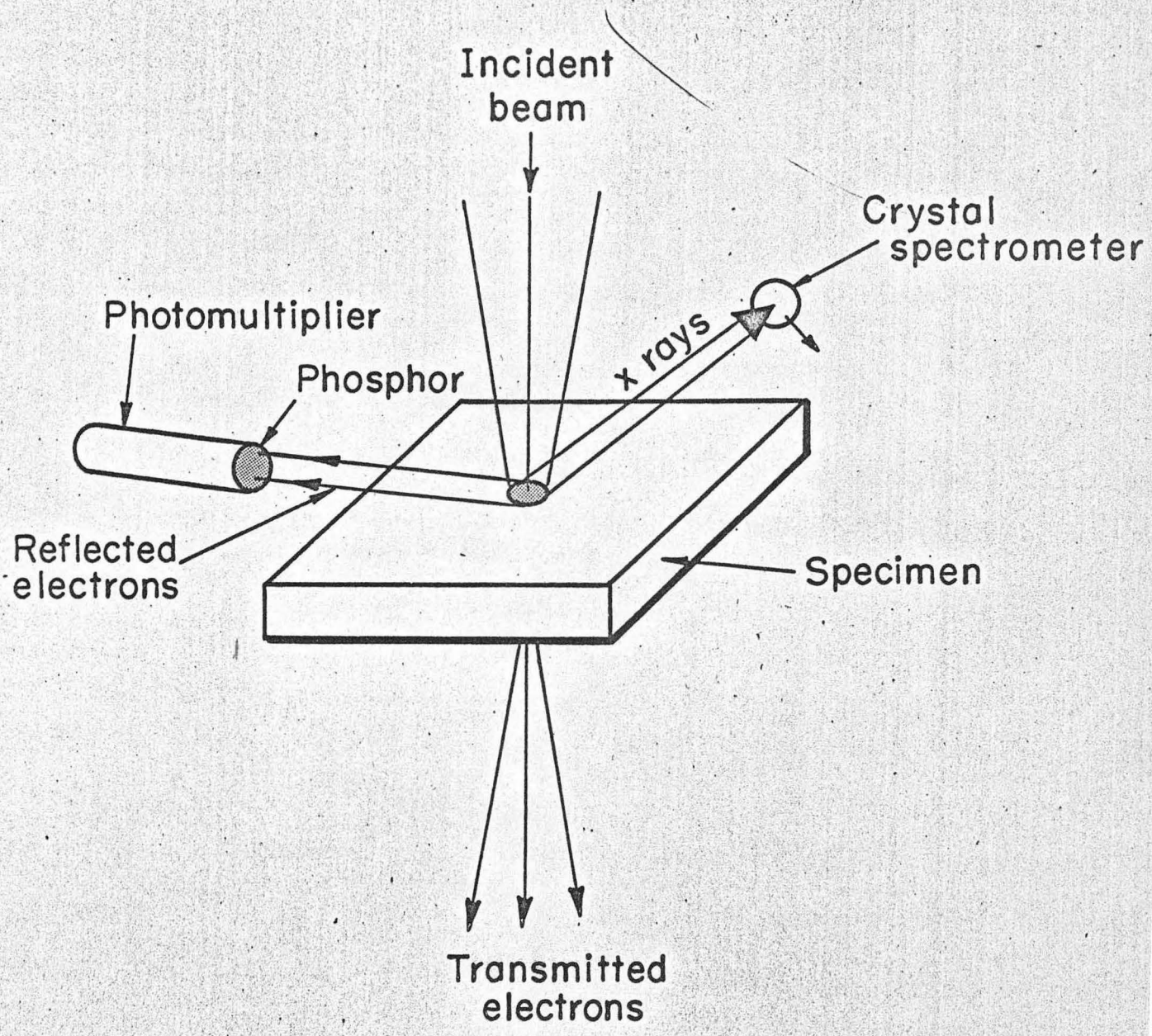
Incident
beam
Crystal
spectrometer
Photomultiplier
Phosphor
x rays
Reflected
electrons
Specimen
Transmitted
electrons
MU-32344

Fig. 27.

TOP

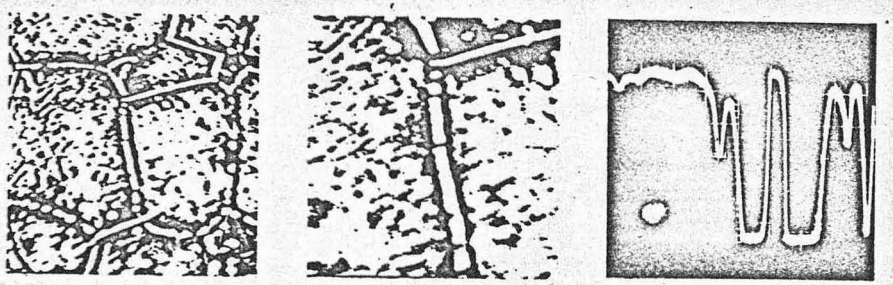

(a) (b) (c)

Figs. 28(a), (b), and (c).

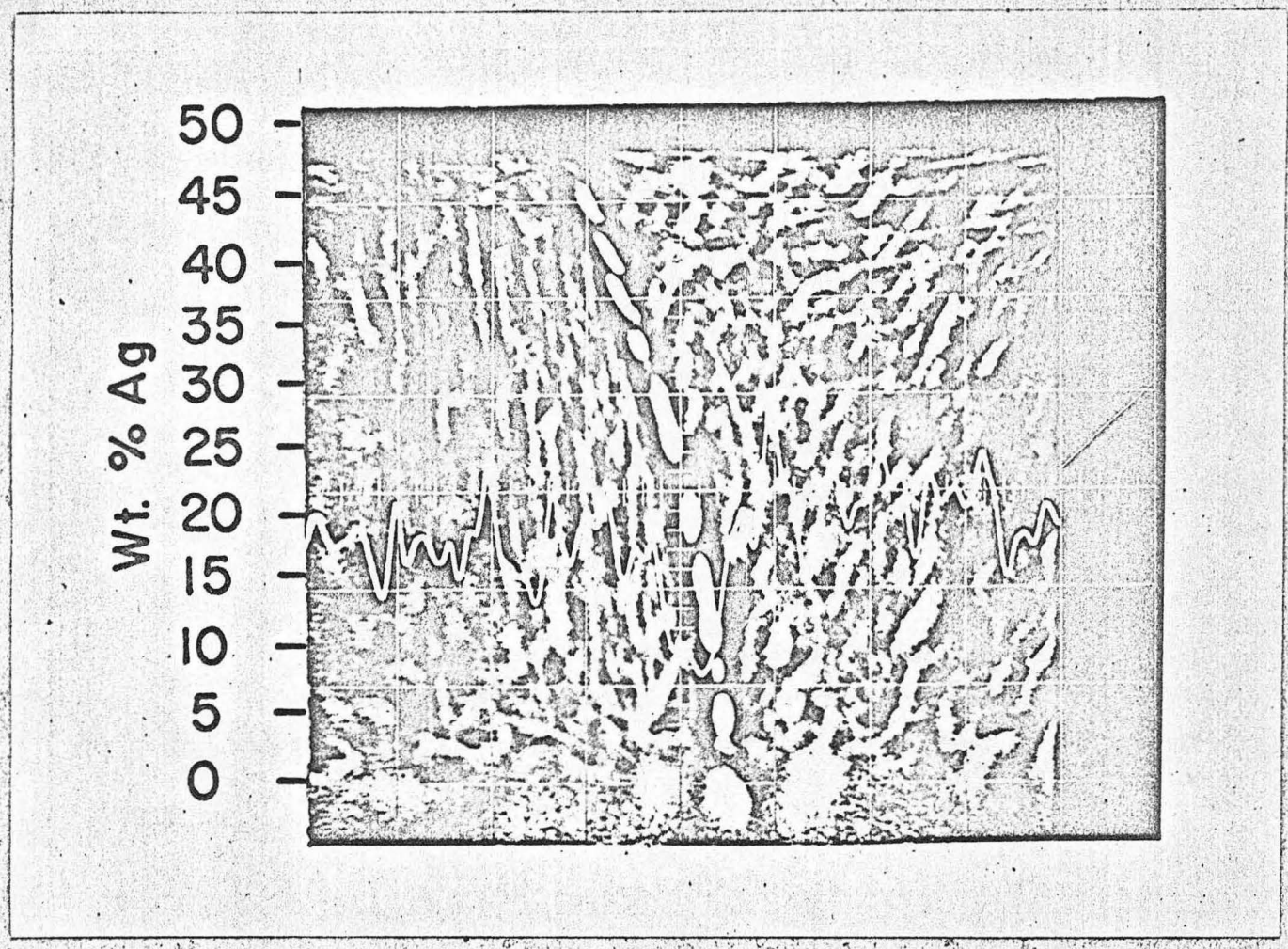

Fig. 29.

NOTE: This Figure 30 was used only in the Journal copy and no other copies are available.

Fig. 30.

NOTE: This Figure 31 was used only in the Journal copy and no other copies are available.

Fig. 31.